NAVAL POSTGRADUATE SCHOOL

MONTEREY, CALIFORNIA

THESIS

TCAD ANALYSIS OF HEATING AND MAXIMUM CURRENT DENSITY IN CARBON NANOFIBER INTERCONNECTS

by

Jason A. Brunton

September 2011

Thesis Advisor:	Todd R. Weatherford
Second Reader:	Sebastion Osswald

Approved for public release; distribution is unlimited

THIS PAGE INTENTIONALLY LEFT BLANK

REPORT DOCUMENTATION PAGE			Form Approved OMB No. 0704–0188
Public reporting burden for this collection of information is estimated to average 1 hour per response, including the time for reviewing instruction, searching existing data sources, gathering and maintaining the data needed, and completing and reviewing the collection of information. Send comments regarding this burden estimate or any other aspect of this collection of information, including suggestions for reducing this burden, to Washington headquarters Services, Directorate for Information Operations and Reports, 1215 Jefferson Davis Highway, Suite 1204, Arlington, VA 22202–4302, and to the Office of Management and Budget, Paperwork Reduction Project (0704–0188) Washington DC 20503.			
1. AGENCY USE ONLY ***(Leave blank)***	**2. REPORT DATE** September 2011	**3. REPORT TYPE AND DATES COVERED** Master's Thesis	
4. TITLE AND SUBTITLE TCAD Analysis of Heating and Maximum Current Density in Carbon Nanofiber Interconnects		**5. FUNDING NUMBERS**	
6. AUTHOR(S) Jason A. Brunton			
7. PERFORMING ORGANIZATION NAME(S) AND ADDRESS(ES) Naval Postgraduate School Monterey, CA 93943–5000		**8. PERFORMING ORGANIZATION REPORT NUMBER**	
9. SPONSORING /MONITORING AGENCY NAME(S) AND ADDRESS(ES) N/A		**10. SPONSORING/MONITORING AGENCY REPORT NUMBER**	
11. SUPPLEMENTARY NOTES The views expressed in this thesis are those of the author and do not reflect the official policy or position of the Department of Defense or the U.S. Government. IRB Protocol number: N/A.			
12a. DISTRIBUTION / AVAILABILITY STATEMENT Approved for public release; distribution is unlimited		**12b. DISTRIBUTION CODE** A	

13. ABSTRACT (maximum 200 words)

As devices shrink, the current density through interconnects increases proportionally making new materials a necessity for industry growth. Carbon nanofiber (CNF) and carbon nanotube's (CNT) potential for high current density make them a possible replacement for metal contacts. Learning the limitations of CNFs and CNTs is important if they are to be used in next-generation electronics. As current density increases, heat is generated throughout the CNF structure. This heating eventually leads to breakdown as the temperature reaches the bonding energy of the Carbon-Carbon (C-C) bond, the bond between two carbon atoms. The resultant reaction is the vaporization of the carbon, eliminating electromigration problems common with metal interconnects.

The physics of breakdown of CNFs is poorly understood. The CNF interconnects' heating under a voltage sweep between two electrodes is modeled in this thesis. A working model was created with Silvaco ATLAS using experimental data provided by Santa Clara University (SCU). An analytical solution was found for the heat generation occurring within the device. The simulation does not show the breakdown occurring; instead, it accurately predicts the temperature and electrical characteristics of the device. This model will aid in the analysis of CNFs' reliability and potential future integration into the next generation electronics.

14. SUBJECT TERMS Carbon Nanotube, CNT, Carbon Nanofiber, CNF, High Current Density, Breakdown, Interconnect, Silvaco ATLAS™, Thermal Breakdown, Reliability, Modeling			**15. NUMBER OF PAGES** 87
			16. PRICE CODE
17. SECURITY CLASSIFICATION OF REPORT Unclassified	**18. SECURITY CLASSIFICATION OF THIS PAGE** Unclassified	**19. SECURITY CLASSIFICATION OF ABSTRACT** Unclassified	**20. LIMITATION OF ABSTRACT** UU

NSN 7540–01–280–5500

Standard Form 298 (Rev. 2–89)
Prescribed by ANSI Std. 239–18

THIS PAGE INTENTIONALLY LEFT BLANK

Approved for public release; distribution is unlimited

TCAD ANALYSIS OF HEATING AND MAXIMUM CURRENT DENSITY IN CARBON NANOFIBER INTERCONNECTS

Jason A. Brunton
Civilian, United States Navy
B.S., University of California at Irvine, 2007

Submitted in partial fulfillment of the
requirements for the degree of

MASTER OF SCIENCE IN ELECTRICAL ENGINEERING

from the

NAVAL POSTGRADUATE SCHOOL
September 2011

Author: Jason A. Brunton

Approved by: Todd R. Weatherford
Thesis Advisor

Sebastion Osswald
Second Reader

Clark Robertson
Chair, Department of Electrical and
Computer Engineering

THIS PAGE INTENTIONALLY LEFT BLANK

ABSTRACT

As devices shrink, the current density through interconnects increases proportionally making new materials a necessity for industry growth. Carbon nanofiber (CNF) and carbon nanotube's (CNT) potential for high current density make them a possible replacement for metal contacts. Learning the limitations of CNFs and CNTs is important if they are to be used in next-generation electronics. As current density increases, heat is generated throughout the CNF structure. This heating eventually leads to breakdown as the temperature reaches the bonding energy of the Carbon-Carbon (C-C) bond, the bond between two carbon atoms. The resultant reaction is the vaporization of the carbon, eliminating electromigration problems common with metal interconnects.

The physics of breakdown of CNFs is poorly understood. The CNF interconnects' heating under a voltage sweep between two electrodes is modeled in this thesis. A working model was created with Silvaco ATLAS using experimental data provided by Santa Clara University (SCU). An analytical solution was found for the heat generation occurring within the device. The simulation does not show the breakdown occurring; instead, it accurately predicts the temperature and electrical characteristics of the device. This model will aid in the analysis of CNFs' reliability and potential future integration into the next generation electronics.

THIS PAGE INTENTIONALLY LEFT BLANK

TABLE OF CONTENTS

LIST OF FIGURES

LIST OF TABLES

THIS PAGE INTENTIONALLY LEFT BLANK

LIST OF ACRONYMS AND ABBREVIATIONS

ITRS	International Technology Roadmap for Semiconductors
CNT	Carbon Nanotube
CNF	Carbon Nanofiber
SWCNT	Single-Walled Carbon Nanotube
MWCNT	Multi-Walled Carbon Nanotube
SCU	Santa Clara University
Si	Silicon
SiO_2	Silicon Dioxide
SiC	Silicon Carbide
Au	Gold
W	Tungsten
Cu	Copper
CVD	Chemical Vapor Deposition
SEM	Scanning Electron Microscopy
K	Kelvin
TCAD	Technology Computer Aided Design
C-C	Carbon-Carbon
0D	Zero-Dimensional
1D	One-Dimensional
2D	Two-Dimensional
3D	Three-Dimensional
cm	Centimeter
μm	Micrometer
nm	Nanometer
J_{max}	Maximum Current Density

THIS PAGE INTENTIONALLY LEFT BLANK

EXECUTIVE SUMMARY

The purpose of this work was to develop a device simulation that would accurately model the maximum current density and the heating within a carbon nanofiber (CNF) interconnect. A CNF is a type of carbon nanotube (CNT) that is one possible material that may replace copper interconnects in the near future. As such, it is necessary to develop a method for analyzing their capabilities. A successful model would have the ability to identify potential shortcomings and advantages of CNFs as compared to current interconnect technology. Experimentation done by a group at Santa Clara University (SCU) was the basis for developing the technology computer aided design (TCAD) simulation.

The experiments from the SCU group analyzed various breakdown and transport characteristics of CNFs. Unfortunately, they have no method for monitoring the conditions of the device during operation. This group has performed mathematical modeling on their structures; however, the functionality of those models is limited. No simulation has previously been developed to accurately model a CNF device under operation. The Silvaco TCAD products are utilized in this thesis to create a model for prediction of current density and heating effects inside the device. Developing a model that can accurately simulate a CNF allows for faster testing methods and the ability to identify the root causes of failure mechanics.

The device was developed to test CNFs of various lengths under an applied voltage sweep. The device characteristics the SCU group developed during their experimental testing were used to define the thermal and contact model parameters. Using knowledge of CNTs, we incorporated other physics-based characteristics about the device into the model.

CNFs and CNTs are unlike other interconnects because of their geometry. The cylindrical structure of CNFs makes them more difficult to model. As a result, the best approximation of the three-dimensional (3D) structure was converted into a two-dimensional (2D) cross section of the active regions of the device. Multiple length interconnect structures were created for testing. Two main sets of simulations were

performed. One set examined the dependence of maximum current density on the length of interconnect. The other examined the effect of the CNF coming into contact with the substrate material at the center point of the interconnect length. A third simulation compares the heating effects in the 2D cross-section model versus a 3D model of the same device.

Simulations of the structures showed that the model could closely approximate the data achieved experimentally. For longer length interconnects, the data matches the slope of the fitted data from SCU experimentation. Possible causes for the discrepancies are either poorly defined physics of the material or a result of the 2D geometry or both.

While this model may have limited functionality, it provides a starting point for more complex modeling of CNF materials. As the model matures, it would be possible to apply any electrical parameter to the contact to measure the materials response. Utilization of this model could validate the functionality and reliability of CNFs for use in interconnects.

ACKNOWLEDGMENTS

First, I would like to thank my thesis advisor, Dr. Todd Weatherford, for providing his time and guidance. His knowledge and encouragement was indispensable during this thesis process.

I also appreciated the help provided by Santa Clara University, specifically Toshishige Yamada and Cary Yang, who answered questions throughout my research. I would also like to acknowledge Silvaco International's Derek Kimpton and Eric Guichard, who responded to my many questions concerning their product.

Finally, I would like to thank my parents, who provided encouragement and support to me throughout this process. Their support for my continuing education has truly made me thankful to be called their son.

THIS PAGE INTENTIONALLY LEFT BLANK

I. INTRODUCTION

Interconnects are the simplest and the most common components in electronic circuits and, as a result, there are a wide variety of types. According to the International Technology Roadmap for Semiconductors (ITRS), interconnects are one of a list of factors that need to be considered for the future of electronics. The ITRS differentiates interconnects into two categories based on gate length of transistors. These categories are split between the near term and high power applications, greater than 16 nm, and the long term and low power applications, less than 16 nm. As the connection distance decreases different factors become important due to various quantum effects. Interconnects that fall in the near term/high power applications category are considered in this thesis. According to the ITRS, we see that there are five critical factors that contribute to interconnect engineering in this group. They include the type of material used, reliability, metrology, manufacturing integration, and manufacturing efficiency. The first three factors are addressed in this project.

Electronic interconnects currently utilize copper, but there is a strong push to replace them with materials with greater conductivity capabilities. Carbon nanotubes (CNTs) offer these properties as well as the possibility for greater reliability. Researchers at Santa Clara University (SCU) work with CNTs with slightly different properties called carbon nanofibers (CNFs). CNFs are CNTs with non-tubelike structures within their outer shells. SCU has been studying the thermal and transport characteristics of CNFs for the purpose of integrating them into the next generation devices. Because the ability to manufacture these devices has current limitations, the researchers at SCU are only able to make one test sample at a time, which leads to a shortage of usable samples for extensive testing. In actuality, a large number of CNFs are produced when they are grown [1]. The problem is that applying them to a device requires precision, and there is currently no automated process to accomplish this task.

The goal of this project was to recreate some of the experiments done by SCU on these CNFs used as interconnects and create a working computer model that could

predict and analyze the structure. The model was used to analyze maximum current density with respect to structural changes to the CNF interconnect. The results were then used to predict the failure limits of the CNF interconnect material. The use of physics based computer modeling for the study of new material for use as interconnects is demonstrated in this thesis.

A. RESEARCH APPROACH

A semiconductor simulation program to construct a physical model of a CNF interconnect and simulate its operation under various conditions to determine thermal characteristics during operation as well as maximum current density was used in this thesis. The program utilized was Silvaco, which is a suite of programs that work together to perform physics-based simulation studies of semiconductor devices. The primary programs used for this project include DevEdit, DevEdit3D, ATLAS, TonyPlot3D, and TonyPlot. There were multiple iterations to the program in order to create a working model.

The first phase of the project involved creating two-dimensional (2D) and three-dimensional (3D) models of the interconnect device using DevEdit and DevEdit3D, respectively. DevEdit is a program that can graphically define a device, and DevEdit3D is the same except that a third axis of a structure can be defined. DevEdit was the only software tool that allowed the construction of a circular region, which was necessary for the 3D CNF structure. The only way to get the proper dimensions for the 3D device was to draw a cross-sectional view of the device using DevEdit3D. By defining the sizes of the regions in the third dimension, the structure was generated. The mesh, defining where the simulator will solve equations, was also created within DevEdit. Once this iteration was complete, the structure could be viewed in TonyPlot and TonyPlot3D.

In the second phase of the project, the correct materials for each region were defined so the structure would have characteristics similar to its real-world counterpart. All of the material characteristics for the CNF section were modified from values originally associated with silicon carbide (SiC). These changes were all applied in ATLAS.

The third phase involved verifying that the structure and new material parameters could produce results similar to the SCU group. This involved applying a voltage sweep and measuring the current density and temperature. In this final phase, some of the factors examined included length of the CNF and the effect of supporting a portion of the CNF with the substrate. Although the length of the CNF and contacts were changed, the substrate of the device was kept constant to maintain proper scale.

The completed simulations were exported to TonyPlot3D and TonyPlot to analyze the heating in specific sections of the CNF. Since there were simulations from multiple lengths of the CNF, the simulation had to be run individually for each length. The resultant data was used to investigate the dependence of current density and thermal characteristics versus various structural factors of the device.

B. RESEARCH OBJECTIVE

The goal of this thesis was to develop a computer model of a CNF interconnect to investigate the thermal characteristics of a CNF material under various electrical stress. There have been papers published that deal with length and contact material for a DC mode [2–9]. With a computer simulation, it is possible to introduce a variety of input characteristics while maintaining a constant structure. Structural inconsistencies between nanotubes can be a problem that limits testing capability. Because of the size of the devices, it is incredibly difficult to get the kind of detailed measurements that can be generated from a computer model. The research done in [2–11] was only able to determine the breakdown current of the CNFs with respect to length and some basic thermal characteristics. The 2D simulation strived to create something that could closely predict these breakdown characteristics.

C. IMPORTANCE

As with any new technology, it is important to establish limits of operation. Copper is becoming difficult to manage as device dimensions shrink. This means the future of interconnects depends upon new materials and novel ideas. CNTs are one of the most promising to replace copper. Although CNFs are not currently used in

manufacturing, there will be a push for interconnects with higher current density capabilities. Because they are at least one order of magnitude larger than CNTs, CNFs can be a good replacement for larger scale devices that require high current density.

D. THESIS LAYOUT

This thesis is divided into five chapters. Background relevant to working with CNTs and interconnects is provided in the next chapter. The SCU experiments and the development of the models are detailed in Chapter III. In Chapter IV, the experiments are detailed and analyzed. Finally, in Chapter V, the conclusions drawn from the experiments are explained and recommendations for improvements and future projects are provided.

II. BACKGROUND

The three most important things to understand for this project are the many types of carbon nanotube-like structures (allotropes), interconnect technology, and previous simulations of similar structures. To best understand how this element works, it is necessary to examine the simplest structures and work towards the more complex. After analyzing the properties of the various structures, one can see how this material can be incorporated into current interconnect technology.

A. CARBON

Electrical and thermal conductance, mechanical strength, and weight-to-strength ratio are just some of the reasons as to why carbon and, more specifically, CNTs and graphene are of such great interest to the scientific community. CNT's official discovery occurred in 1991 by Sumio Iijima, a Nippon Electric Company (NEC) researcher at the time [12]. The first CNTs were needle-like tubes composed of multiple layers. Iijima had created the first experimentally proven, multi-walled carbon nanotube (MWCNT) [2]. He later discovered single-walled carbon nanotubes (SWCNT) in 1993 [13]. Since Iijima's discovery, study of CNTs has increased enormously. This has led to more research being conducted on the manufacturability of CNTs and the effects of replacing a multitude of current electronic materials with CNTs.

Carbon is the only element that has isomers from zero dimensions (0D) to three dimensions [1]. Even though all the structures are composed of the same element, their properties can vary simply based on their structure. The simplest and perhaps easiest isomer to create is graphene. CNTs are rolled up graphene sheets. CNTs come in two different categories, SWCNTs and MWCNTs. Lastly, you get the CNF which is a MWCNT with variable structures on the interior of the innermost tube. This is the order in which the different structures will be covered.

1. Graphene Properties

a. Structure

Graphite is the most common allotrope of carbon composed of multiple layers of graphene. Graphene consists of a repeating pattern of hexagonal shapes on a planar surface, where each point of the hexagon corresponds to a carbon atom. This means that any carbon atom in the structure has three neighboring carbon atoms to which it is bonded. In Figure 1, the unit cell and Brillouin zone are shown along with unit vectors [1],

$$\vec{a}_1 = \left(\frac{\sqrt{3}}{2}a, \frac{a}{2}\right), \ \vec{a}_2 = \left(\frac{\sqrt{3}}{2}a, -\frac{a}{2}\right), \tag{1}$$

and reciprocal lattice vectors,

$$\vec{b}_1 = \left(\frac{2\pi}{\sqrt{3}a}, \frac{2\pi}{a}\right), \ \vec{b}_2 = \left(\frac{2\pi}{\sqrt{3}a}, -\frac{2\pi}{a}\right), \tag{2}$$

where a is defined as the lattice constant of the carbon structure.

In Figure 1b, the triangle ΓMK, shown by the dotted line, determines the region being solved for the energy dispersion relations. These points are important for determining physical characteristics later.

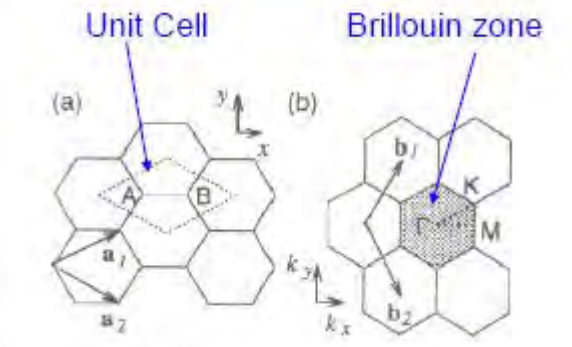

Figure 1. (a) The unit cell and (b) Brillouin zone are defined for a graphene sheet. After [1]

b. Physics

A carbon atom contains four bonds, three σ-bonds that hybridize in a sp^2 configuration and a $2p_z$ orbital [1]. The σ-bond is the strongest form of covalent bond. These kinds of bonds are formed by direct overlapping between atomic orbitals. The $2p_z$ orbital is perpendicular to the graphene plane, creating a π covalent bond. A π-bond is an indirect covalent bond. These bonds usually occur between two barbell-shaped parallel *p* orbital shells. The bonding is indirect because the shared electron clouds do not overlap the nucleus of the atom and, as a result, are much weaker [1].

The three σ bonds are used to bond the atom to adjacent carbon atoms. As a result, the π bond becomes the most important for determining the solid state properties [1]. The energy dispersion relations for the π-bond and the π* anti-bonding band are illustrated in Figure 2. The points in Figure 2 correspond to the Brillouin points seen in Figure 1b.

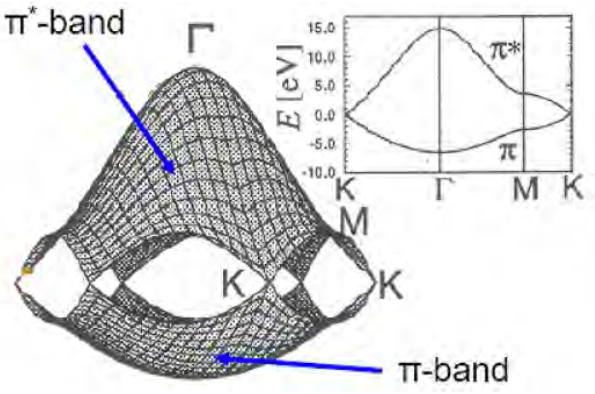

Figure 2. The energy dispersion relations for 2D graphite are shown for the Brillouin zone. The inset graphs the energy dispersion along the high symmetry directions of the triangle ΓMK shown in Figure 1. After [1].

According to Saito *et al* [1], since there are two π electrons per unit cell, these two π electrons fully occupy the lower π band. A detailed calculation shows that the density of states at the Fermi level is zero. This means that two-dimensional graphite is a zero-gap semiconductor. The existence of a zero gap at the *K* points gives rise to quantum effects in the electronic structure of carbon nanotubes [1]. A simple approximation for the electronic structure of a graphene layer is provided by [1] as:

$$E_{g2D}(k_x, k_y) = \pm t\left\{1 + 4\cos\left(\frac{\sqrt{3}k_x a}{2}\right)\cos\left(\frac{k_y a}{2}\right) + 4\cos^2\left(\frac{k_y a}{2}\right)\right\}^{1/2}. \quad (3)$$

The variables k_x and k_y correspond to the x and y directions of the wavevector $\vec{k}$. Equation 3 is used to obtain a simple approximation for the electronic dispersion relations for carbon nanotubes. This dispersion relation is very important for calculating the energy dispersion and electronic structure for CNTs.

2. CNT Properties

a. Structure

As its name suggests, carbon nanotubes are tube-like structures composed of carbon atoms or, more specifically, graphene sheets of carbon atoms. CNTs come in two different varieties, SWCNT and MWCNT. The SWCNT has only one layer of graphene rolled into a tube-like shape, whereas MWCNT have multiple layers. The number of layers creates a drastic difference in the properties and physics of the structures [1].

CNTs are classified into three categories based on their symmetry: armchair, zigzag, and chiral. The first two classifications are achiral, which means that any nanotube with these structures has a mirror image with an identical structure to the original tube. The method for classifying nanotubes involves determining its chiral vector C_h. The parameter C_h can be expressed by the unit vectors a_1 and a_2 of the hexagonal lattice defined as [1]:

$$C_h = na_1 + ma_2 \equiv (n, m), \ (n, m \text{ are integers}, 0 \le |m| \le n). \quad (4)$$

The absolute value of C_h, L, corresponds to the circumference of a cross section of a nanotube. The variables n and m are used to define what kind of tube has been made. When $n = m$, an armchair nanotube is created. A zigzag nanotube is created when $m = 0$. Any other combination of n and m will generate a chiral nanotube. The difference between these structures can be seen in Figure 3.

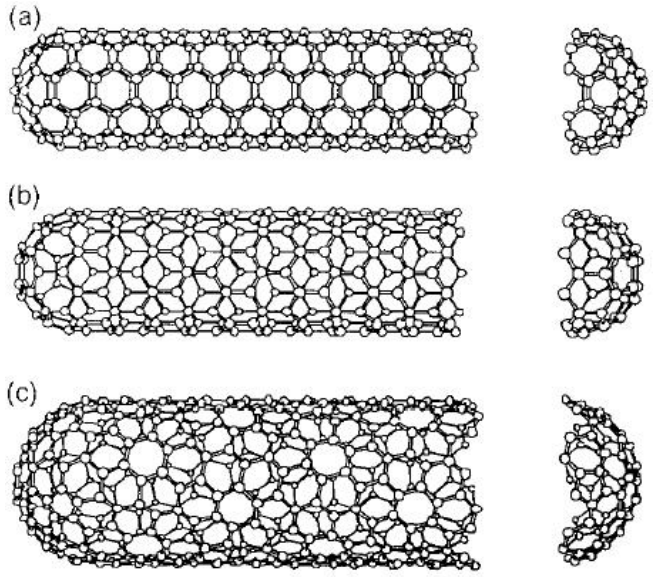

Figure 3. Classification of carbon nanotubes: (a) armchair, (b) zigzag, and (c) chiral nanotubes. From [1].

Once C_h is defined, the diameter of the nanotube d_t can be calculated from [1]

$$d_t = L/\pi,\ \mathrm{L}=\left|C_h\right| = \sqrt{C_h \cdot C_h} = a\sqrt{n^2+m^2+nm}. \tag{5}$$

Another important vector that defines a nanotube is the translational vector T. The vector T is normal to the chiral vector and is defined to be the unit vector of a one-dimensional (1D) carbon nanotube by [1]:

$$\mathbf{T} = t_1 a_1 + t_2 a_2 \equiv (t_1, t_2),\ \text{(where } t_1, t_2 \text{ are integers)}. \tag{6}$$

The variables t_1 and t_2 are defined as [1]:

$$t_1 = \frac{2m+n}{d_R},\ t_2 = -\frac{2n+m}{d_R} \tag{7}$$

where d_R is the greatest common divisor of $(2m + n)$ and $(2n + m)$. With the vectors T and C_h, the 1D unit cell can be defined. When the vector product operator is applied to the two vectors and divided by the area of a hexagon, the number of hexagons per unit cell N is obtained defined by [1]:

$$N = \frac{\left|C_h \times T\right|}{\left|a_1 \times a_2\right|} = \frac{2\left(m^2+n^2+nm\right)}{d_R} = \frac{2L^2}{a^2 d_R}. \tag{8}$$

Thus, there are $2N$ carbon atoms in each unit cell of the carbon nanotube [1].

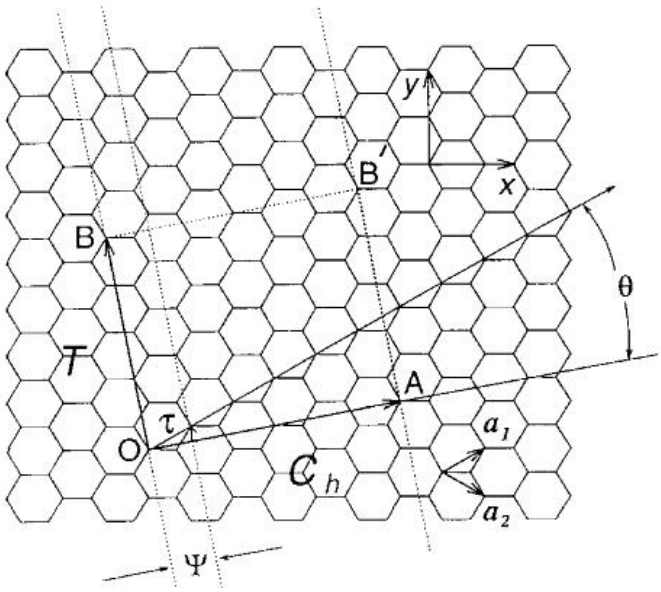

Figure 4. The unrolled honeycomb lattice of a nanotube with C_h = (4, 2). From [14].

How vectors *T* and C_h would look on a graphene sheet is illustrated in Figure 4. When points *O* and *A* are connected and *B* and *B`* are connected, a nanotube can be constructed. The resultant nanotube is defined as C_h = (4, 2). This is determined by using the unit vectors a_1 and a_2.

Though there are other parameters that are used to define carbon nanotubes, most of them are not important for basic understanding. Table 1 is a complete list of all the parameters of CNTs. However, once C_h and *T* are determined, all the other values can be calculated from them.

All of these parameters play a role when determining the physics of an individual CNT. The parameters that are the most important are the *n* and *m* values and the resulting diameter of the CNT. With these two parameters, the electrical characteristics of the CNT can be calculated.

Table 1. Parameters for carbon nanotubes are shown. From [14].

Symbol	Name	Formula	Value
$a_{C\text{-}C}$	carbon-carbon distance		1.421 Å (graphite)
a	length of unit vector	$\sqrt{3}a_{C\text{-}C}$	2.46 Å
$\mathbf{a}_1, \mathbf{a}_2$	unit vectors	$\left(\frac{\sqrt{3}}{2}, \frac{1}{2}\right)a, \left(\frac{\sqrt{3}}{2}, -\frac{1}{2}\right)a$	in (x, y) coordinates
$\mathbf{b}_1, \mathbf{b}_2$	reciprocal lattice vectors	$\left(\frac{1}{\sqrt{3}}, 1\right)\frac{2\pi}{a}, \left(\frac{1}{\sqrt{3}}, -1\right)\frac{2\pi}{a}$	in (x, y) coordinates
$\mathbf{C}_h$	chiral vector	$\mathbf{C}_h = n\mathbf{a}_1 + m\mathbf{a}_2 = (n, m)$	n, m: integers
L	circumference of nanotube	$L = \lvert\mathbf{C}_h\rvert = a\sqrt{n^2 + m^2 + nm}$	$0 \le \lvert m\rvert \le n$
d_t	diameter of nanotube	$d_t = \frac{L}{\pi} = \frac{\sqrt{n^2 + m^2 + nm}}{\pi}a$	
θ	chiral angle	$\sin\theta = \frac{\sqrt{3}m}{2\sqrt{n^2 + m^2 + nm}}$	$0 \le \lvert\theta\rvert \le 30°$
		$\cos\theta = \frac{2n + m}{2\sqrt{n^2 + m^2 + nm}}$	
		$\tan\theta = \frac{\sqrt{3}m}{2n + m}$	
d	the highest common divisor of (n, m)		
d_R	the highest common divisor of $(2n + m, 2m + n)$	$d_R = \begin{cases} d & \text{if } n - m \text{ not a multiple of } 3d \\ 3d & \text{if } n - m \text{ a multiple of } 3d. \end{cases}$	
$\mathbf{T}$	translational vector of 1D unit cell	$\mathbf{T} = t_1\mathbf{a}_1 + t_2\mathbf{a}_2 = (t_1, t_2)$	t_1, t_2: integers
		$t_1 = \frac{2m + n}{d_R}$	
		$t_2 = -\frac{2n + m}{d_R}$	
T	length of $\mathbf{T}$	$T = \frac{\sqrt{3}L}{d_R}$	
N	number of hexagons per 1D unit cell	$N = \frac{2(n^2 + m^2 + nm)}{d_R}$	$2N = n_C$/unit cell
$\mathbf{R}$	symmetry vector‡	$\mathbf{R} = p\mathbf{a}_1 + q\mathbf{a}_2 = (p, q)$	p, q: integers†
		$d = mp - nq,\ 0 \le p \le n/d,\ 0 \le q \le m/d$	
M	number of 2π revolutions	$M = \lvert(2n + m)p + (2m + n)q\rvert/d_R$	M: integer
		$N\mathbf{R} = M\mathbf{C}_h + d\mathbf{T}$	
R	basic symmetry operation‡	$R = (\psi \mid \tau)$	
ψ	rotation operation	$\psi = 2\pi\frac{M}{N}, \left(\chi = \frac{\psi L}{2\pi}\right)$	ψ: radians
τ	translation operation	$\tau = \frac{d\mathbf{T}}{N}$	τ, χ: length

† (p, q) are uniquely determined by $d = mp - nq$, subject to conditions stated in table, except for zigzag tubes for which $\mathbf{C}_h = (n, 0)$, and we define $p = 1$, $q = -1$, which gives $M = 1$.
‡ $\mathbf{R}$ and R refer to the same symmetry operation.

b. Physics

The physics behind carbon nanotubes can get quite complicated and, in some cases, are far more involved than is needed for this project. The physics that are necessary for effectively defining this project are covered in this section. There are two main points that must be covered. The first important point is the method for determining if a CNT is metallic or semi-conductive. The second involves defining the general electrical structure of CNTs.

One of the unique properties of CNTs is that they can be either metallic or semi-conductive depending on their structure. The effect of chirality in determining if the nanotube is metallic or semi-conductive is illustrated in Figure 5.

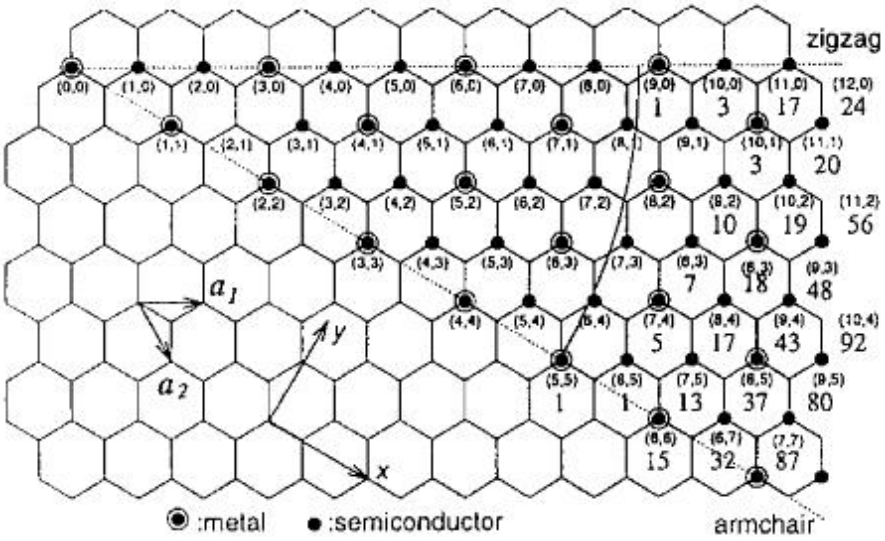

Figure 5. The electronic structure of a CNT given the chirality vector. One third of the vectors possible produce metallic nanotubes. The remaining nanotube combinations are semi-conductive. From [14].

This ratio of metallic to semi-conductive nanotubes becomes especially important when dealing with MWCNT. Since about one third of the cylinders of a MWCNT are conducting, certain electronic properties, such as the electrical conductivity of nanotubes, will be dominated by the contributions from the conducting constituents, and the non-conducting constituents will play almost no role [1]. This is a very crucial point for this project because we are dealing with MWCNT-like structures.

Because this project deals exclusively with MWCNT, only the electronic structure of metallic nanotubes is covered here. As such, it is important to know how and why a metallic CNT forms. The condition for metallic energy bands in a CNT is illustrated in Figure 6a.

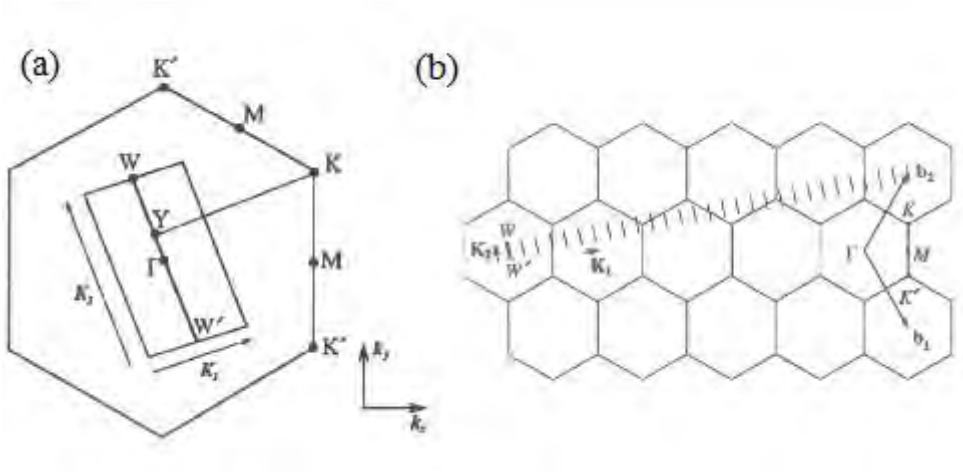

Figure 6. (a) The condition for metallic energy bands is shown. (b) The multiple Brillioun zones of a CNT are shown. From [1].

The vectors K_1 and K_2 are defined as [1]:

$$K_1 = \frac{1}{N}(-t_2 b_1 + t_1 b_2),\ K_2 = \frac{1}{N}(m b_1 - n b_2), \tag{9}$$

where b_1 and b_2 are defined in equation 2 and t_1 and t_2 are defined in equation 7. The term N is defined in equation 8 and also defines the number of Brillouin zones. In Figure 6a, the line $WW`$ corresponds to the first Brillouin zone of this one-dimensional material. The vector $K_2$ defines the length of the $WW`$ line. The K_1 vector defines the distance between subsequent Brillouin zones up to N iterations. The many Brillouin zones of a carbon nanotube with a C_h = (4, 2) is illustrated in Figure 6b.

The Brillouin zone is important for determining whether or not the nanotube has metallic properties. According to the energy dispersion of the π-bands shown in Figure 2, the Brillouin zone has zero band gap at the vertexes of the hexagon. In Figure 6a, those same points correspond to K and $K`$.

The condition for obtaining a metallic energy band is that the ratio of the length of the vector $\overrightarrow{YK}$ to that of K_1 in Figure 6a is an integer. Since the vector $\overrightarrow{YK}$ is given by [1]:

$$\overrightarrow{YK} = \frac{2n+m}{3} K_1, \tag{10}$$

the condition for metallic nanotubes is that $(2n+m)$ or equivalently $(n-m)$ is a multiple of three [1]. This is the reason why one third of nanotubes end up being metallic. Once a nanotube is determined to be metallic or semi-conductive, the electronic structure of the CNT can be defined.

The electronic structure of metallic CNTs is fairly straightforward. At finite temperatures, the band gap of the CNT is zero. This means that very little energy is required to excite electrons into the conduction band. Also, for all metallic nanotubes, independent of their chirality and diameter, it follows that the density of states per unit length along the nanotube axis is a constant given by [1]:

$$N(E_F) = \frac{8}{\sqrt{3}\pi a|t|}, \tag{11}$$

where a is the lattice constant of the graphene layer and $|t|$ is the nearest neighbor Carbon-Carbon (C-C) tight binding overlap energy [1]. This means there are a finite number of states for conduction.

An important characteristic pertaining to semiconducting nanotubes is the energy gap. The energy gap of semiconducting nantubes depends upon the reciprocal nanotube diameter d_t [1],

$$E_g = \frac{|t| a_{C-C}}{d_t}, \tag{12}$$

independent of the chiral angle of the semiconducting nanotube, where $a_{C-C} = a/\sqrt{3}$ is the nearest-neighbor C-C distance on a graphene sheet [1]. This means that as the diameter of the nanotube increases, the band gap of the CNT decreases. Therefore, since this project deals with MWCNT and large diameter CNTs, the band gap of devices is

very small or zero even for the semi-conductive nanotube shells. All of these properties are the same for CNFs with some slight differences.

3. CNF Properties

CNFs are MWNTs that are slightly more complicated than CNTs in that they have large diameters and variable internal structures. CNFs are between 25–200 nm, which is one to two orders of magnitude greater than most SWCNT and MWCNT. From equation 12, these large diameters imply that the bandgap for the semi-conductive CNT shells will be at or near zero. Any nanotube with a diameter greater than 14 nm has a bandgap comparable to the thermal activation energy [1].

Aside from the multiple outer walls, CNFs have internal structures composed of failed nanotubes. Failed nanotubes are graphene shells that might be at an inverted angle, so that instead of creating a tube, a cone is generated. In some cases, a tube-like structure is created, but it does span the entire length of the nanotube. This kind of structure is refered to as bamboo-like. The difference between a regular nanotube and the internal nanofiber structure is illustrated in Figure 7. When the term $\alpha=0$, the structure maintains a tube-like structure, but as α increases, cone shaped structures begin to form.

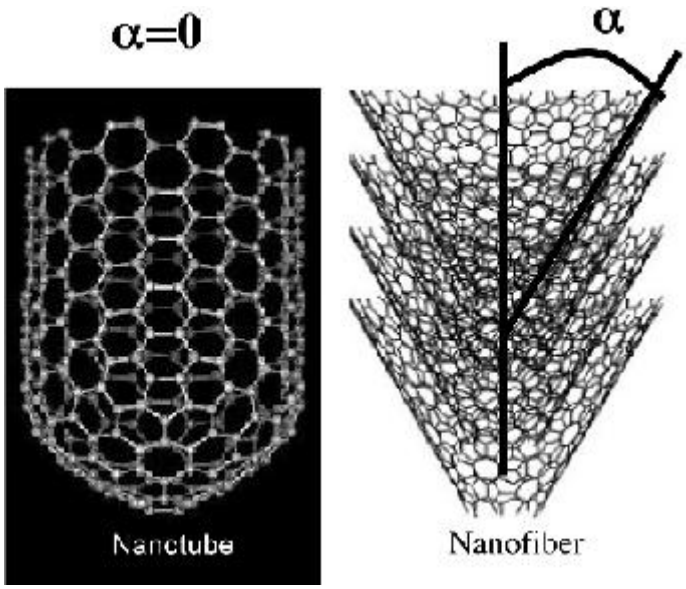

Figure 7. Comparison of nanotube and nanofiber structures is shown. From [15].

In normal MWCNT, the interior of the structure is empty, which means there is no conduction through this region. CNFs do have these interior structures but, because the distance between the layers is so large, electrons still primarily conduct along the exterior of the CNF layers. There can be thermal conductivity through this interior region that will contribute to the overall thermal coefficient. The thermal features and pertinent physics of the CNF structures are covered in more detail when the SCU experiments are discussed. Another important feature of CNFs is that they are easier to create then the more ordered CNTs.

4. CNT/CNF Synthesis Methods

As mentioned earlier, the first nanotubes were discovered by accident by Sumio Iijima as a byproduct of one of his experiments [12]. Carbon nanotubes can be grown in a variety of ways. The method for growth determines what kind of CNTs are created. Some methods are more effective at producing particular kinds of CNTs. Since they were first discovered, many new methods have been developed. Some of these methods include chemical vapor deposition, arc discharge, and laser ablation.

a. Chemical Vapor Deposition (CVD)

CVD is the most widely studied method because of its ability to produce CNTs continuously. CVD is the method used by the SCU group to make their CNFs. If the proper conditions are defined, this method could be a very good way to synthesize large quantities of CNTs under controlled conditions [1].

The growth process for CNTs involves the use of a catalyst metal to begin the formation of CNT structures. Some of the metals used are nickel (Ni), iron (Fe), and cobalt (Co). In order to grow CNTs, any one of these metals are patterned on a substrate and placed in a reaction chamber. Then the chamber is heated up to about 1100 C, and hydrocarbon gases are pumped in. The gases react with the metal catalysts, slowly depositing carbon atoms with a hexagonal lattice. The leftover hydrogen atoms are flushed from the chamber by more incoming hydrocarbons. The catalization process and the synthesis of CNTs are illustrated in Figure 8.

The resulting nanofibers are primarily MWCNT with some SWCNT present. Due to their low energy formation, the structures have poor crystallinity until they are heat-treated. There have been improvements to this method that involve the use of plasma to facilitate catalyzation.

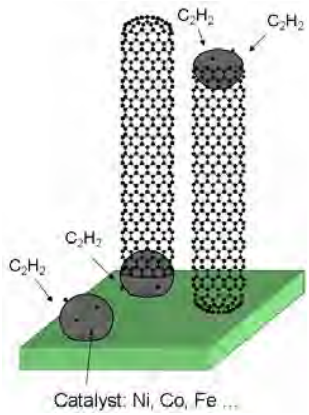

Figure 8. CVD catalyzation process is shown. From [16].

b. Arc Discharge

The arc discharge method uses a different approach to generate CNTs. Typical conditions for operating a carbon arc for the synthesis of CNTs include the use of carbon rod electrodes separated by a small distance with a voltage across the electrodes and a dc electric current flowing between the electrodes [1]. Carbon begins to deposit on the negative electrode. This method has the ability to make both MWCNTs and SWCNTs. No catalyst is needed to create the MWCNT. SWCNTs can be grown using similar catalyst to those used for the CVD method. This method creates limited quantities based on the carbon electrode used since the carbon electrode transforms into the nanotubes.

c. Laser Vaporization

Laser vaporization is an efficient method for synthesizing bundles of SWCNTs. This method is performed by placing a Co-Ni/graphite target in a heated flow tube, and then two sequenced laser pulses are used to evaporate the target. Flowing

argon gas removes the entrained nanotubes from the high temperature region and deposits them into a water-cooled Cu collector downstream. By varying growth parameters, the average nanotube diameter and diameter distribution can be varied [1].

B. INTERCONNECT TECHNOLOGY

1. Current Interconnects

Currently, Cu is the primary material used for interconnects in devices. Cu has been in use for over a decade as interconnects, but new problems are emerging as the industry moves forward. During a period in which the reliability of Cu-based interconnects is expected to rapidly decrease, the reliability requirements per unit length is rapidly increasing [16]. As devices shrink, new materials are needed to overcome the problems associated with current metal interconnects. The problems most commonly encountered are maximum current density, electromigration, resistance, and signal delay.

As devices shrink, the current density through interconnects increases proportionally, making new materials a necessity for industry growth. The maximum current densities recorded for Cu interconnects are on the order of 10^{6}–10^{7} A/cm^{2}. The copper interconnect is now routinely used with minimum feature sizes down to 130 nm [17]. When interconnect dimensions reach the nanometer range, the maximum current densities do not allow for large potential differences between contacts and breakdown occurs much more quickly.

Another factor that can cause interconnects to fail is electromigration. Electromigration is the transport of atoms from one physical location to another on metal interconnects. As atoms move from one point on an interconnect to another point, thinning occurs at one end of the device, and current density in that region increases rapidly. As interconnect dimensions decrease, the current density associated with a given voltage increases, causing an eight-fold increase in the electromigration rate with every halving of the line width (for a fixed thickness-to-width ratio) [16].

Resistivity in Cu interconnects is also a problem as feature dimensions shrink. The scattering of electrons by surfaces and grain boundaries leads to increased resistivity

as line widths are decreased [16]. This resistance becomes much more noticeable for long interconnects. As a result of the resistance increase, there is much greater signal delay in large scale devices. The proposed alternative to Cu interconnects is CNT and CNF interconnects.

2. CNF Advantages

CNTs and CNFs have numerous advantages over metal interconnects, making them an important material to consider as a replacement. In nearly all the above categories, CNTs outperform Cu interconnects.

One of the most important selling points of CNTs is that they have the potential for much higher current densities ($10^{8-}10^{10}$ A/cm^2) [17–19]. These densities are two to three orders of magnitude greater than those found in Cu. A contributing reason for this difference is that a CNT's mean free path is in the micrometer range compared to the ~40 nm mean free path of Cu [20]. The large mean free path allows ballistic transport through the CNT. Ballistic transport results in reduced resistivity and strong atomic bonds, which provide tolerance to electromigration [20].

Electromigration occurs differently in CNT interconnects than it does in metal interconnects. Instead of metal from the interconnect material moving from one site to another, a CNT interconnect transports metal between the contact points of the CNT. Electromigration occuring on a CNT is illustrated in Figure 9. Even though electromigration still occurs, it is greatly reduced as a result of the ballistic transport of the CNT.

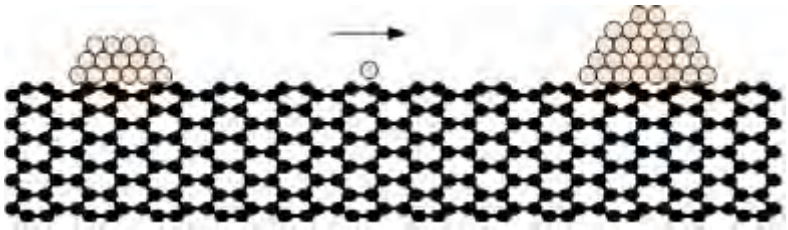

Figure 9. Electromigration of metal on a CNT is shown. Atoms move along the surface of the CNT. From [16].

In addition, the resistivity of the CNT is smaller because of the ballistic transport. This leads to long CNTs offering significantly reduced resistance compared to Cu [16]. For the most part, in shorter length interconnects the resistances are comparable.

Because of increased potential current density and decreased electromigration effects and resistance, CNTs can be used in smaller device structures with fewer negative effects. Overall, CNTs and CNFs provide a possible alternative to Cu for future interconnect technology.

C. PREVIOUS WORK

There have been numerous groups that have made models for CNTs. Only one is covered in this work. The model covered provides an equivalent circuit of a metallic MWCNT interconnect. With this model certain assumptions can be made about the basic electrical characteristics of a metallic MWCNT and, therefore, CNFs.

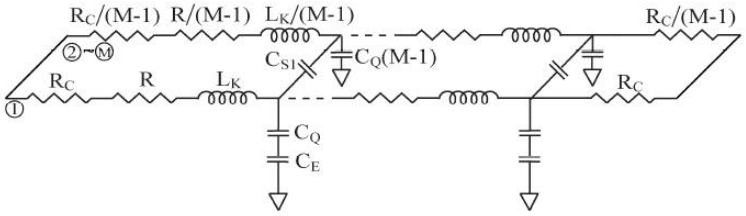

Figure 10. Simplified equivalent circuit of a metallic MWCNT interconnect. From [20].

The work by Srivastava *et al* [20] derives an equivalent circuit for metallic MWCNTs. In their model they consider factors such as the number of walls and contact resistances. The simplified circuit is illustrated in Figure 10 [20].

The terms C_E and C_Q correspond to series and parallel capacitances, respectively, between shells. The term R_C is the contact resistance, and the term M is the number of shells. The kinetic inductance per unit length L_K, quantum capacitance per unit length C_Q, and resistance R are the terms that define the electrical properties of any given shell. This model simplifies further into Figure 11 [20].

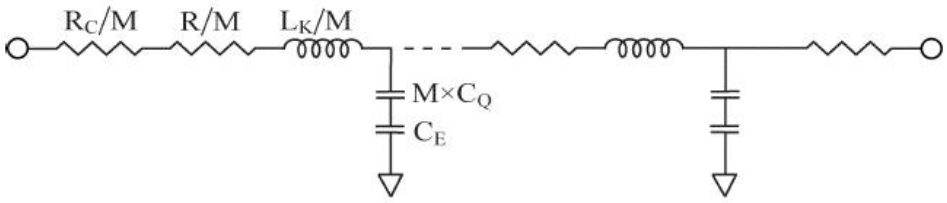

Figure 11. Simple equivalent circuit model of a metallic MWCNT interconnect. From [20].

When M is large, C_Q can be neglected, which means the capacitances of a MWCNT interconnect is smaller than that of a SWCNT. In addition, the resistance and inductance of all metallic shells are parallel and M times smaller than that of a SWCNT [20]. Using this information, we see that a CNF also has small values for its resistance, capacitance, and inductance [20].

D. CHAPTER SUMMARY

In this chapter, carbon materials and structures, interconnects, and previous work modeling CNTs were examined. It was determined that carbon has many structural parameters that determine if the CNT/CNF is metallic or semi-conductive. Some of these parameters are dependent on the growth methods used. It was found that interconnect technology could greatly benefit from the addition of CNTs as a replacement for current Cu interconnects. The previous work examined another group who has created models of CNT interconnects.

In the next chapter, the SCU experiments are analyzed. Also, an introduction to the Silvaco simulation software and its implementation for creating the test structures are examined.

THIS PAGE INTENTIONALLY LEFT BLANK

III. DEVICE AND SIMULATION

In this chapter, the procedure for creating the simulation is covered. The first step to accomplishing this was to define the parameters for the experiment. As discussed previously, the work done by the group at SCU was the inspiration for creating the model and was used extensively to define the CNF parameters of the device. In the following section, the SCU experiments are detailed and the information extracted was defined.

The second part of this chapter provides details about the simulation software and the generated model. The basics of Silvaco's programs are covered along with a description of the process for creating structures and defining device properties. Then, using data from the SCU experiments, test parameters were input and the model was finalized for testing and verification.

A. SCU EXPERIMENTS

1. Overview

The primary method of verification for this project was based on the work done by Santa Clara University [2–11]. They conducted numerous experiments on basic carbon nanofiber interconnects to determine their breakdown characteristics. Some of the characteristics that they studied include temperature dependence, the composition of the contacts, length dependence, transport phenomena, and the effect on the CNF while in contact with the substrate. Multiple structures were implemented in order to test all of these parameters.

The basic device is composed of a silicon dioxide (SiO_2) substrate with two gold contacts separated by a distance of microns. The two gold contacts are about 100 nm thick and connected by a CNF. The lengths of the CNFs vary between 1.5–8.6 μm and have diameters of between 100–200 nm [2]. The CNFs in these experiments are grown using the plasma-enhanced chemical vapor deposition method with Ni catalyst. All of the devices were measured to their breakdown limit by current stressing. The primary test parameter studied was the current density through the device because it is closely

related to the amount of joule heating being generated. The four structures that were tested by the group at SCU are illustrated in Figure 12. The Au contact by itself with suspended and supported structures, respectively, are illustrated in Figure 12a and 12b. The W-Au contact with suspended and supported structures, respectively, are illustrated in Figure 12c and 12d. For each set, a scanning electron microscope (SEM) image and a simple structural representation are displayed.

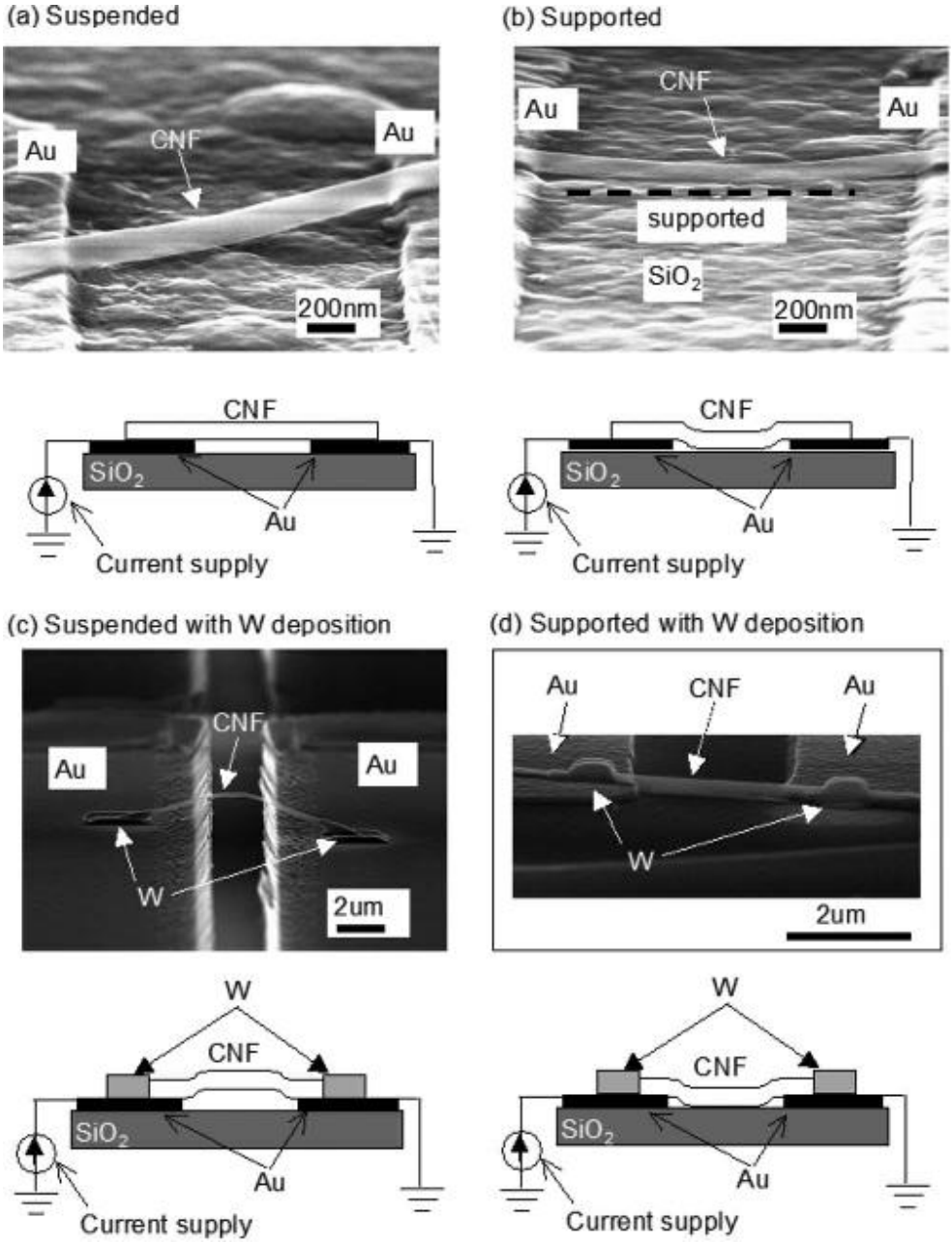

Figure 12. Test structures and SEM images from SCU experiments. From [2].

In some of their experiments, Yamada *et al.* [2–6] examined the effects of laying the CNF so that it came in contact with the substrate, as shown in Figure 12b and 12d. The CNF can either be completely suspended over the SiO_2 substrate or partially in contact with it. The term S is defined as the ratio of the length in contact with the SiO_2 substrate to the CNF interelectrode length. When S = 0, the CNF is completely suspended, and when S = 1, it is completely supported by the substrate. Because the primary method of failure is assumed to be caused by Joule heating, heat can diffuse into the substrate when the CNF comes in contact with the substrate. This contact increases the resulting current density possible through the CNF structure. When breakdown happens, it was proposed that oxidation of the carbon occurs [5].

Another factor that the group at SCU experimented with was the effect of different contacts on the contact resistance and thermal breakdown of the CNF interconnects. Contact resistance was a major factor in a number of the papers. The reason for this is that Au has difficulty bonding to the CNF, creating large resistance values. In order to decrease this contact resistance, the group used current annealing. Current annealing is the process of applying a set amount of current through the interconnect, with the intention of eliminating defects. The initial resistance at the contact is on the order of MΩ. It was found that after about three rounds of the current annealing process, the contact resistance bottomed out with a resistance in the kΩ range [7]. The W-Au contact interconnects did not benefit from this current annealing; however, the addition of the W created a better initial contact, with a resistance in the kΩ range. For this project, only the W-Au contact interconnects were examined. The next section covers the test data that was used to create and verify the output of the simulation.

2. Test Data

The simulations in this thesis achieved an approximate match to the test data shown in Figure 13. The maximum current density versus inverse interconnect length is illustrated in Figure 13. There are three different measurement sets based on the structure at the contacts: suspended CNFs with Au electrodes (solid circles), and suspended (solid triangles) or SiO_2-supported (open triangles) CNFs with W-Au electrodes [2].

The fitted curves are based on the one-dimensional heat transport equation [3–5],

$$\frac{d^2\Delta T(x)}{dx^2} - a^2\Delta T = -bJ^2,\ b = \frac{1}{\kappa\sigma}, \tag{13}$$

where J is the current density and a is the dissipation factor measuring the effectiveness of the heat dissipation to the contact material with units of inverse length. The term ΔT is the local CNF temperature at x measured from the ambient temperature. Finally, the term b equals $1/(\kappa\sigma)$, where κ is the thermal conductivity and σ is the electrical conductivity [3]. In equation 13, the left half of the equation, heat diffusion and heat dissipation, generally depends on location, whereas the right side, heat generation, does not. The temperature of the devices wre estimated through a thermogravimetric measurement [5].

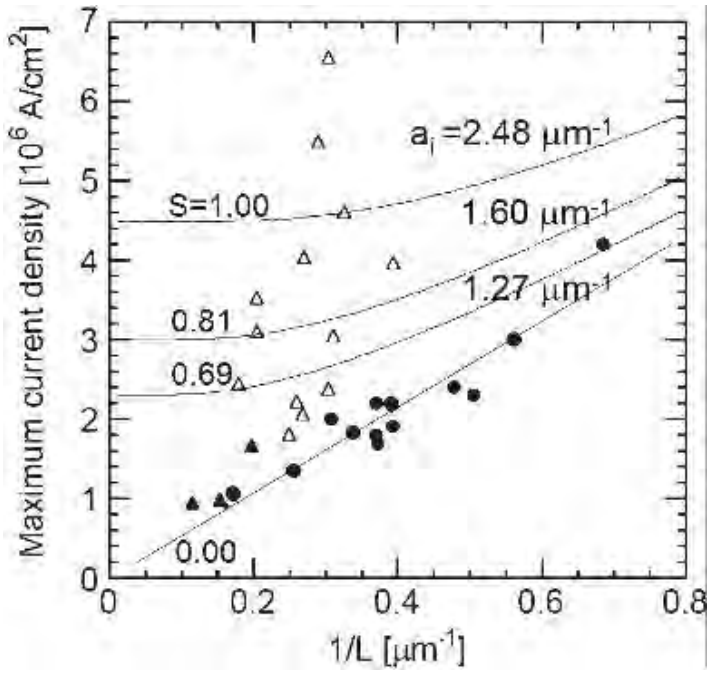

Figure 13. Measured maximum current density as a function of reciprocal CNF length is shown. From [3, 5].

The next section incorporates the experimental data from these experiments into an ATLAS simulation.

B. CNF ATLAS SIMULATION

1. Silvaco Simulation Software

The simulation software suite used for this project was provided by Silvaco International. The software suite is comprised of many different programs that are designed for simulating electronic devices. The programs used for this project from the software suite include ATLAS, Deckbuild, DevEdit, DevEdit3D, TonyPlot, and TonyPlot3D.

The ATLAS device simulator was used for the modeling of the CNF interconnect. ATLAS is a specialized programming language that allows a user to create a physical model of an electronic device. The user can define the structural parameters and physics of the model. ATLAS allows up to 20,000 nodes and 100,000 nodes when solving 2D and 3D simulations, respectively. A node is a point on the structure of the device where the differential equations for electrical and thermal models are solved and convergence is tested for the solutions. All of these nodes together create a mesh. The mesh for this work was defined using the DevEdit program and is described later.

Convergence of solutions can be a constant problem when performing simulations. Some methods to reduce the possibility of problems are to optimize the meshing, determine the best step size when biasing, and to use the proper numeric method. ATLAS has the capability of using multiple methods for obtaining solutions. The Newton solution method obtains solutions for coupled equations, whereas the Gummel method solves the decoupled equations. The Block method is a hybrid of the two. The Block method solves faster than Newton, but may not obtain a solution that is as accurate as Newton method [21]. The user has the ability to choose a combination of the methods to increase the chances of convergence. For this project, the Newton and Block methods were used for the 2D simulations, and a hybrid solver called Halfimplicit was used for the 3D simulation.

When solving for particular parameters in devices, ATLAS has groups of equations that are activated. The group of equations that are used for temperature

calculations are defined as GIGA. ATLAS GIGA self-heating simulator incorporates models for mobility, self-heating effects, and lattice temperature [21]. ATLAS has built-in default values for the material parameters. The user has the ability to define all of the parameters present in the equations to accurately simulate the material's thermal properties.

Deckbuild is a text editor and runtime environment that allows the user to run and modify ATLAS programs. The other programs used are described as they are encountered.

2. Device Construction

In order to accurately construct the device, the programs DevEdit and DevEdit3D were utilized. Both programs provide the ability to draw cross-sections of the device. In DevEdit, the user has the ability to define polygon shapes and map them out on a coordinate plane. DevEdit also allows the user to define the mesh and can automatically generate a mesh for the structure.

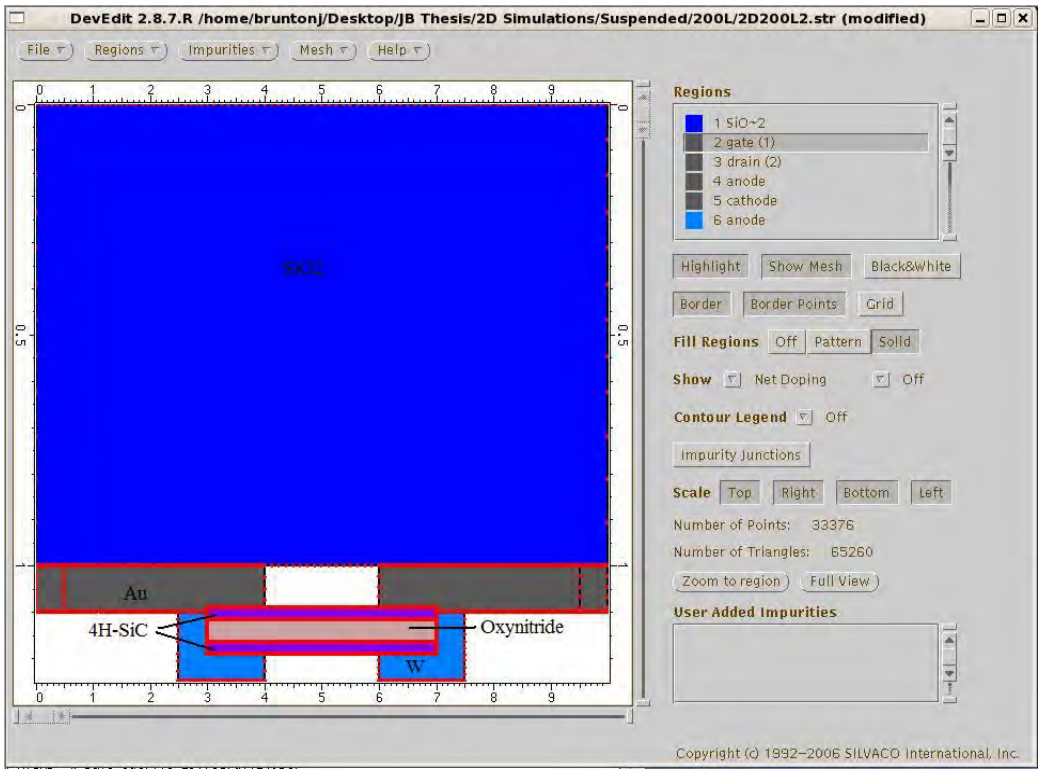

Figure 14. Basic DevEdit model (2.0 µm).

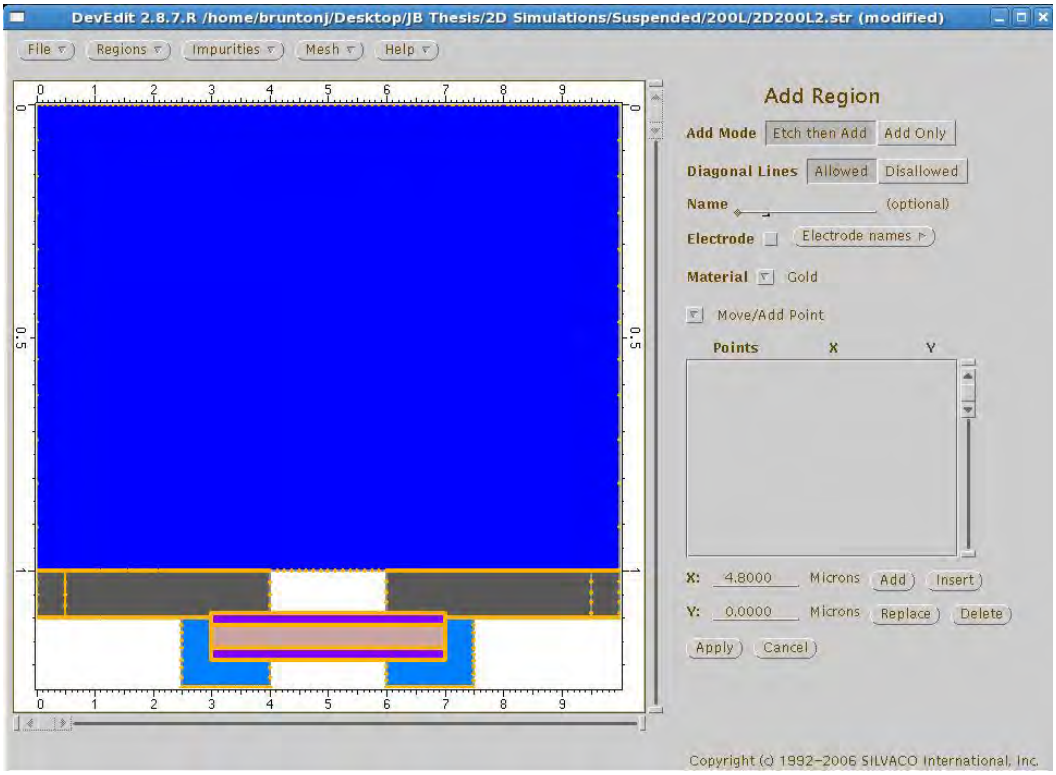

Figure 15. DevEdit Region menu sidebar.

In Figure 14, the basic window for both DevEdit programs can be seen with one of the device structures drawn. It should be noted that the origin of the graph is at the top left corner, which makes the device seem like it is upside down with the active region at the bottom of the figure. At the time of this project, both DevEdit and DevEdit3D only function on a machine running Red Hat Linux OS.

The commands for making a new structure are very straightforward. The first step is to create a new region by using the region drop down menu. Once selected, a new sidebar pops up that allows the user to give a name to the region, define the material, and create the shape of the region. Figure 15 is provided as a reference for defining a region.

The shape of the region can be created two different ways. The first method is accomplished by inputting the points of a polygon or shape underneath the polygon box on the right sidebar. The user needs to remember to hit the enter key, so that the program registers the change to any point values. For the second method, the user simply draws the shape of the region by clicking where on the coordinate plane they wish to place the

points. The program automatically generates lines between points and defines the structure in the polygon window in the right sidebar.

Once all the regions are in place, the mesh for the structure can be created. The user has the option of using the built in meshing ability of DevEdit or manually defining the mesh structure after the structure is brought into ATLAS. The built-in meshing ability was used for this project. Special attention was given to the auto mesh constructed for the device because it was necessary for making the device converge and accurately simulating the device physics.

The particular structures developed are described next, including all the region definitions and the mesh construction.

a. 2D Structure

For the purpose of this project, two distinct drawings were created. The 2D models needed to be drawn as a cross-section of the CNF splitting it along its length. This device is shown in Figure 14. The large section in the figure is the substrate material. If this were a real device, the substrate would be two orders of magnitude thicker. This difference in substrate thickness does impact the thermal properties and is addressed later under the thermal contact condition part of this chapter.

The other materials in Figure 14 are the gold and tungsten contacts and the CNF materials. The important thing to note about the contacts is that the tungsten is required to test this device in 2D. Without it, the multiple materials that the CNF is composed of are not connected, and the outer layer would contribute nothing to the simulation. Since the tungsten contact is required for the 2D simulations, only structures with W-Au contacts were tested.

The CNF structure was defined by three separate regions. There were two regions of material that made up the outer walls of the CNF. Between these two regions was an insulating layer of material that corresponds to the interior structure of the CNF. An insulating layer was chosen because there was no electrical conduction through the center of the CNF, but there was thermal conduction taking place. The lengths of these regions

were always equivalent for every length of CNF tested. Since there is no material that currently has the properties of a CNF, 4H-SiC was chosen as the material to modify for the exterior and Oxynitride was chosen for the interior. The important parameters of the material were changed, so it did not matter which materials were used.

Multiple structures were generated with the primary focus being on creating longer interconnect lengths. This involved shrinking the gold contacts while maintaining the same amount of contact with the CNF structure. As a result, the length of the CNF materials increase as the gap between the gold contacts increases. A total of six different 2D structures were generated for the length dependence tests. The lengths were chosen so as to best fit the testing data from SCU.

Another testing group was created by using three of the above structures and adding in a block of substrate material that connected the center of the CNF to the main substrate. The TonyPlot software is used to illustrate a structure with 25% of the span supported by the substrate in Figure 16. The three different lengths were tested with 25% and 50% of their length supported. The contact was always placed at the center point of the CNF. A complete set of structures generated is shown in Table 2.

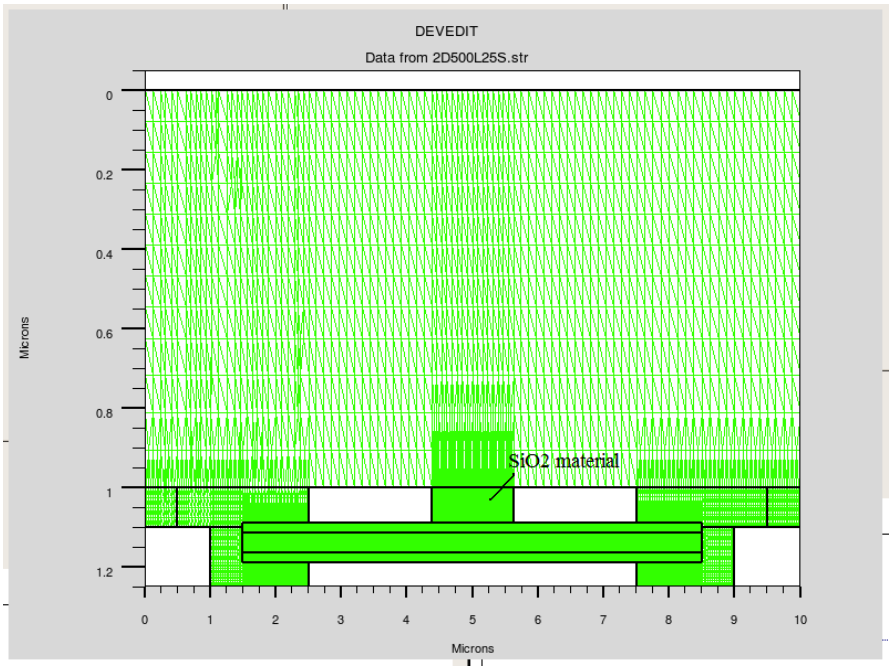

Figure 16. TonyPlot image of five micron interconnect meshed with 25% contact with substrate.

Table 2. List of 2D structures created for simulations.

Length (μm)	1.25	1.75	2.00	2.50	3.75	5.00
Suspended	Yes	Yes	Yes	Yes	Yes	Yes
Supported (25%)	Yes	No	No	Yes	No	Yes
Supported (50%)	Yes	No	No	Yes	No	Yes

The mesh for these structures was generated by the built in meshing function. In order to refine the mesh in the places of greatest interest, new mesh constraints needed to be defined. Mesh constraint definitions determine the distance between solve points. The user can specify constraints for particular groups of materials or individual materials. Only the maximum height and maximum width were modified to obtain mesh definition for this project. The mesh was focused on the CNF materials and contacts. All the mesh constraints applied to the 2D structures are contained in Table 3. A smaller number in Table 3 corresponds to a more defined region of the structure.

Table 3. Mesh constraints for the 2D structures are shown.

Material	Max. Height (μm)	Max. Width (μm)
SiO_2 (substrate)	0.15	0.15
Gold (Au)	0.025	0.05
Tungsten (W)	0.025	0.05
4H-SiC (CNF)	0.005	0.005
Oxynitride (CNF)	0.005	0.005

When importing the DevEdit file into ATLAS, the width of the device needed to be determined. Even though the structure is technically 2D, in order for the simulation to solve properly, a third dimension needs to be defined for the device. For these simulations, the default width of one micrometer was chosen. It should be noted that the resulting structure looks nothing like a CNT/CNF. The CNF layers will look like rectangular blocks. However, since the primary characteristic being measured was

current density, the geometry of the simulated device was not as important as the material characteristics. For the most accurate structural representation of the device, a 3D model was created.

b. 3D Structure

A cross-sectional picture of the 3D structure needed to be drawn to create the radial dimension of the CNF. The cross-section for the 3D device is illustrated in Figure 17. It should be noted that DevEdit is the only program in the Silvaco suite of products that allows the creation of circular regions in conjunction with rectangular regions.

Any circle or arc created using DevEdit is actually a polygon with a set number of sides. The program allows the user to define how accurately they want the curved region to resemble a circle. For this experiment, the greatest accuracy was used, which places a point at every degree for a total of 360 points. The drawback to choosing this highly defined structure was that the mesh structure needed to be extremely refined around the boundary points of the CNF structure. This circular pattern was used for both regions of the CNF section. The internal region was composed of an insulator with a diameter of 50 nm, and the outer layer had a thickness of 25 nm, thus giving the CNF a diameter of 100 nm.

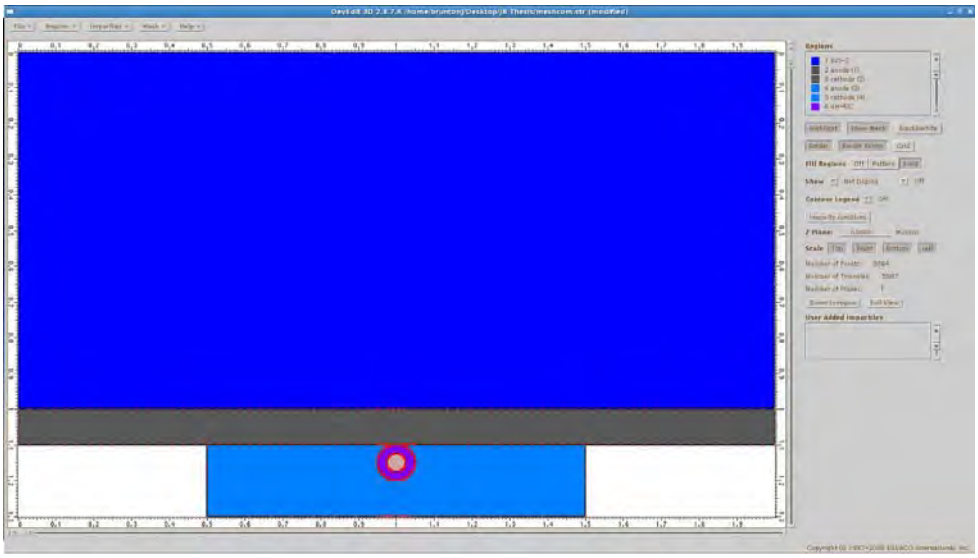

Figure 17. Cross-section of 3D device with circular CNF.

The key difference between DevEdit and DevEdit3D is the ability to define the third dimension of a device. This is done by defining the *z*-dimension to various depths. One thing to note is that if the user closes the program and then goes back to edit the structure, all of the *z*- dimension values must be input again. This issue also applies to the mesh constraints defined for either DevEdit programs.

The 3D model was not as extensively tested as the 2D simulations. There was only one model created for the purpose of determining the heating characteristics in a geometrically accurate CNF.

3. Material Properties

The primary focus of this project was to design a simulation that could approximate the qualities of a CNF material. In order to accomplish this, a known material needed to be modified to have the same characteristics found in a CNF. The parameters that were changed included the band, recombination, and thermal parameters. All changes to the characteristics occur within the ATLAS code.

The material chosen to be modified was 4H-SiC. It was chosen because 4H-SiC is not as common as other materials such as Si within the ATLAS code. As a result of extensive testing, some materials, such as Si, defined in ATLAS have a more refined set of characteristics that if modified can generate errors in the simulation. Since insulators have very few parameters that contribute to a simulation, Oxynitride was chosen as the interior insulating material.

The band parameters of the 4H-SiC material were the greatest contributing factor to the material characteristics. As discussed previously, CNFs are MWCNTs with an irregular internal structure. Since MWCNT are always metallic, the CNF materials had to be metallic. However, as a result of the imperfect formation process, electron traps occur in the structure causing the CNF to exhibit semi-conductive qualities. In order to account for this property, the two conducting regions were defined as semiconductors with a band gap equal to the thermal activation energy (~26 mV). With such a small band gap, the material still acted like a conductor but allowed the user to have greater control over the physics in the material. This control was very important for measuring

the current density. If the material had been defined as a conductor, the ATLAS simulation would not have produced current density as an output.

The other band parameters that played a role were the density of states and the permittivity. The density of states has enormous effects on the breakdown of the device. As stated earlier in the text, metallic CNTs have a finite density of states. Therefore, the density of states for the CNF materials was set at a constant value according to equation 11. The permittivity of both CNF materials was estimated based on the permittivity of similar carbon materials. For this simulation, the permittivity of diamond was used.

Although there may be some recombination occurring due to traps, the primary heating method for the device was from Joule heating. Instead of trying to account for an unknown number of traps, the recombination parameters in the device were all set to zero. This might have caused some slight error in the finished simulation; however, any error should have been negligible compared to the Joule heating effect.

The thermal parameters were taken directly from the experimental data. ATLAS calculates heat based on the lattice heat flow equation [21]

$$C\frac{\partial T_L}{\partial t} = \nabla(\kappa \nabla T_L) + H, \tag{14}$$

where C is the heat capacity per unit volume, κ is the thermal conductivity, H is the heat generation, and T_L is the total lattice temperature. In general, the thermal conductivity is temperature dependant. ATLAS acknowledges this by having multiple models that are available for use. According to the SCU data, the thermal and heat conductivity of the CNF material are constant. The data was unclear about which portion of the CNF the conductivity data applied to. As a result, both the active and passive regions of the CNF were defined with these conductivity values.

Table 4. Passive region (Oxynitride) material parameters changed are shown.

Type of Parameter	**ATLAS identifier**	**Changed Value**
Band Parameter	Permittivity	5.4
Thermal Parameter	tc.const	0.12
	HC.A	1.75
	HC.B, HC.C, HC.D	0

Table 5. Active region (4H-SiC) material parameters changed are shown.

Type of Parameter	**ATLAS identifier**	**Changed Value**
Band Parameter	Permittivity	5.4
	EG300	0.026
	NC300, NV300	$3x10^{17}$
	NC.F, NV.F	0
Recombination	taun0, taup0	0
Parameters	nsrhn, nsrhp	0
	ksrhtn, ksrhtp	0
	ksrhcn, ksrhcp	0
	ksrhgn, ksrhgp	0
	augn, augp	0
	augkn, augkp	0
	kaugcn, kaugcp	0
	kaugdn, kaugdp	0
	Etrap	0
	Copt	0
Thermal Parameters	tc.const	0.12
	HC.A	1.75
	HC.B, HC.C, HC.D	0

A complete list of the parameters and their changed values are shown in Tables 4 and 5. The band parameters affect the band structure of the device. The term permittivity defines the permittivity of the device. The term EG300 defines the bandgap of the structure. The rest of the terms in the band parameters section of Table 5 control the density of states. The initial density of states in the conduction and valence band are defined by the terms NC300 and NV300, respectively. The terms NC.F and NV.F are an exponential factor that modifies the density of states with respect to temperature. These were chosen to be zero because the density of states needed to remain constant.

The thermal parameters HC.A, HC.B, HC.C, and HC.D affect the heat conduction of the device and tc.const specifies a constant thermal conductivity value.
The recombination parameters in Table 5 are all zero and are not defined because they do not contribute to the simulation. If traps were being considered as another possible heat source, the terms etrap, taun0, and taup0 would be given values. The general code used to implement these changes into the model is contained in the Appendix.

4. Thermal Contact Conditions

The SiO_2 layer on the bottom of the device was much thicker than the CNF and contact layers. The substrate of the device was two orders of magnitude thicker than the device modeled. Since this excess material only makes a thermal contribution to this model, it can be replaced by an equivalent thermal contact.

Within the ATLAS program, it is possible to define a thermal contact in the thermocontact statement with the parameter α. From the ATLAS User's Manual [21], α is determined from the thermal resistance of the material as shown by,

$$R_{TH} = \frac{1}{\alpha},\ \alpha = \frac{k\pi}{2S}, \tag{15}$$

where k is the thermal conductivity and S is the surface length from a point on the interface to some radius. The term α is measured in W/cm^2-K. Equation 15 implies that the thermal resistance is determined by the ratio of the width to the cross-sectional area. Since the thermal conductivity of SiO_2 is known, only the geometry of the represented region was needed.

The geometry of the substrate region was calculated by using the three-dimensional model, where the substrate surface was 20 μm^2 and the depth of the substrate was 200 μm. The thermal resistance of a substrate with this geometry was calculated to be 1400 W/cm^2-K. The contact was placed at the bottom 100 nm of the substrate. It was assumed that in all cases the same amount of excess substrate would be present. Therefore, this value was used for both the 2D and 3D simulations. The implementation of this contact can be seen in the Appendix.

5. Simulation Parameters

In order to run the ATLAS code, there are other device characteristics that needed to be defined. The first parameters that needed to be given values were the contact resistances. Once the resistances were defined, the bias conditions were established.

Contact resistances were applied to the electrode contacts to simulate the resistances seen in the SCU experiments. The electrode contacts were placed at the very edge of the device as part of the gold contacts. The placement isolated the electrical bias from regions with potentially large temperature gradients. The resistances applied to the electrodes were in the low kΩ range. These resistance values corresponded to the best electrical contacts that were achieved by the SCU group. No resistance was given to the CNF material but rather incorporated into the contact resistances at the electrodes. This is a valid assumption if the transport is considered to be ballistic [11].

A basic voltage sweep was determined to be the most effective bias for driving the device. A voltage sweep is an incrementally increasing applied voltage to an electrode contact over a specific range measuring a parameter. For low voltages, step sizes were kept the same. As the voltage increased, the different structural lengths reached their maximum current densities at different potentials. Therefore, the end voltage of the sweep was determined based on the demands of the individual structures. More specific information about biasing values is provided in Chapter IV under the relevant sections of each structure. The implementation of the bias can be viewed in the Appendix.

C. CHAPTER SUMMARY

In this chapter, the basics of the SCU experiments and an overview of the construction of the simulation were covered. From the SCU experiments, the test data showed that as the interconnect length decreases, the maximum current density increases. Also, heat accumulated in the center of suspended regions of the device.

The Silvaco software and implementation of the SCU experimental data into the simulation was also covered in this chapter. A total of thirteen structures were generated for testing. The material parameters of the CNF materials were presented and explained. Finally, a brief explanation was given for some of the other simulation parameters.

In the next chapter, the simulation data is analyzed and compared to the SCU experimental data. The chapter is broken up into three main sections. The first two sections deal with the 2D structures' heating characteristics and current densities. The heating in a 3D structure is compared to that in a 2D structure of similar length in the last section.

THIS PAGE INTENTIONALLY LEFT BLANK

IV. EXPERIMENTATION AND RESULTS

Using the devices and structures discussed in Chapter III, we biased the device structures using a voltage sweep with the goal of determining the maximum current density of the simulated material. The maximum current density (J_{max}) versus length with W-Au contacts was examined in the first group of experiments. The effect of having the center of the CNF in contact with substrate was examined in the second group of experiments. Finally, in order to verify the heating characteristics of the device, a 3D simulation was run and compared to its 2D equivalent.

A. 2D SUSPENDED W-AU CONTACT

1. Device Structures

A total of six different lengths of CNF interconnects were created for comparison with the SCU experimental data. The lengths chosen included 1.25, 1.75, 2.00, 2.50, 3.75, and 5.00 μm. These lengths were chosen to give the best range of values that correspond to the experimental data from SCU. The measure of length corresponds to the distance bridged by the CNF between the two gold contacts. It does not represent the physical dimensions of the CNF material. The 2D device structure was discussed in greater detail in Chapter III.

2. Voltage Sweep

Each device structure was simulated with a voltage sweep. The two characteristics studied included the heating and the current density within the device. The voltage steps were kept the same for all the different lengths of CNF. However, as the length increased the device reached its maximum current density at a lower voltage. This meant the maximum voltage was limited by the length of the device. The voltage was increased until a maximum current density was reached.

a. Heating of Device

The heating in all six device structures is shown in Figures 18 through 23. The figures are presented in order of increasing length. In all cases, the center of the interconnect heated up the fastest.

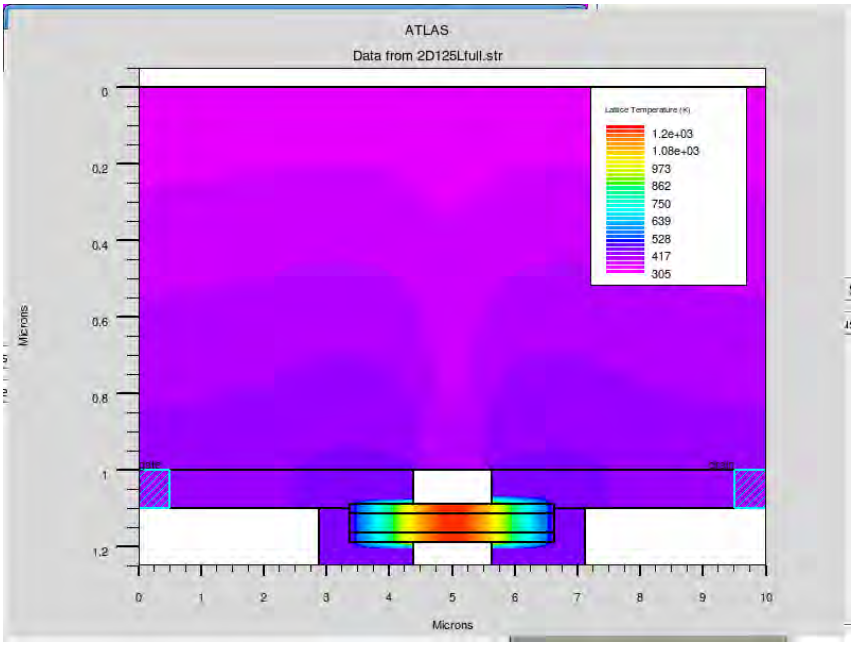

Figure 18. Heating in a suspended 1.25 µm CNF interconnect.

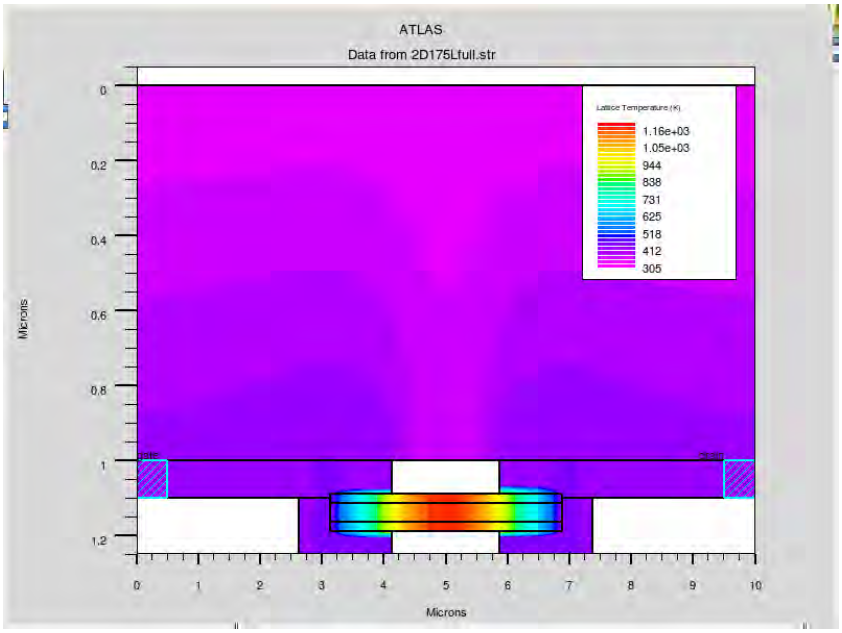

Figure 19. Heating in a suspended 1.75 µm CNF interconnect.

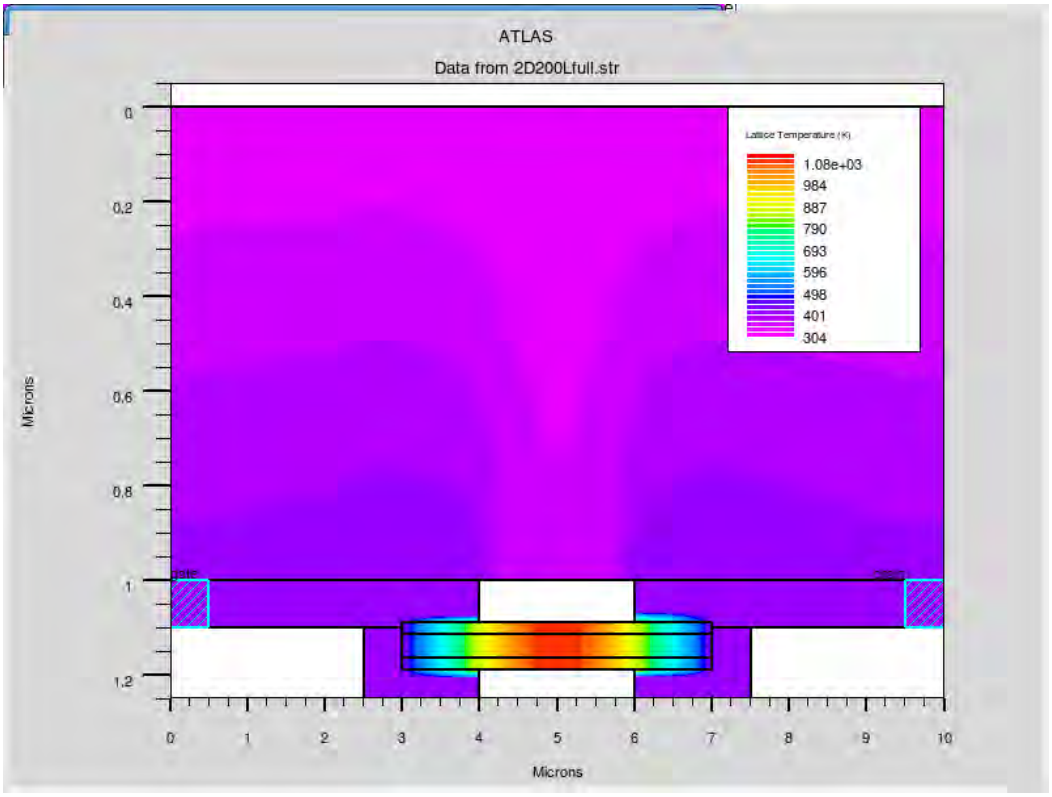

Figure 20. Heating in a suspended 2.00 µm CNF interconnect.

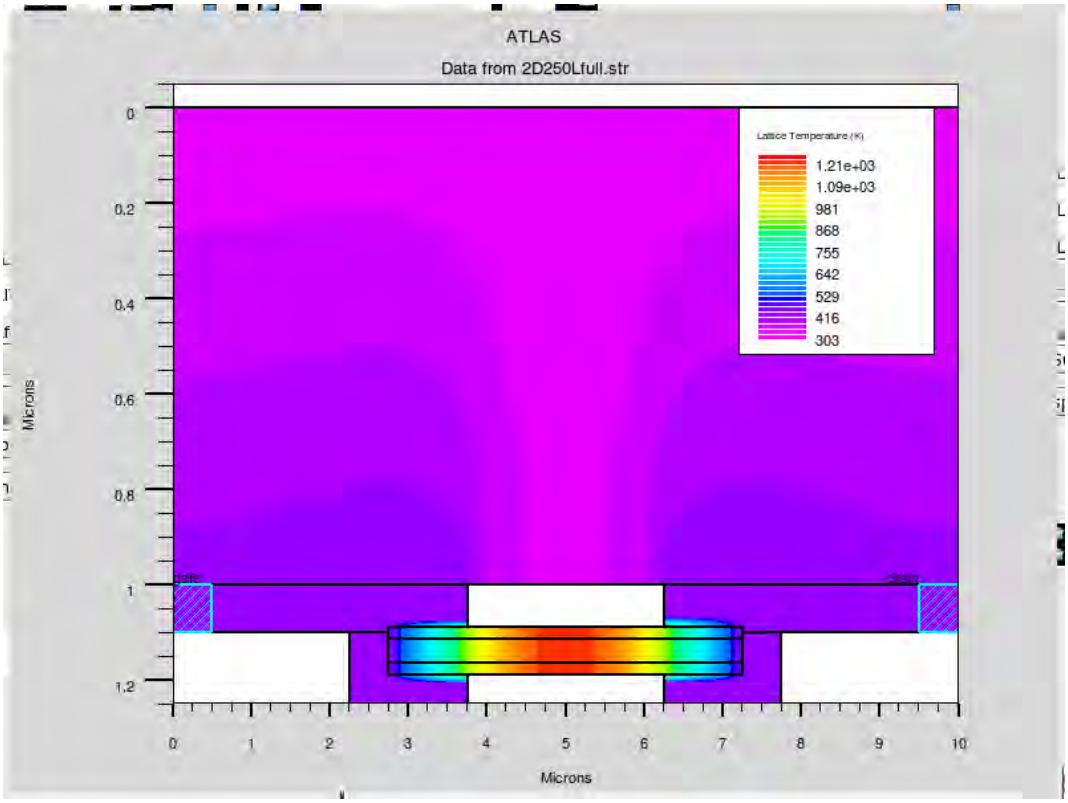

Figure 21. Heating in a suspended 2.50 µm CNF interconnect.

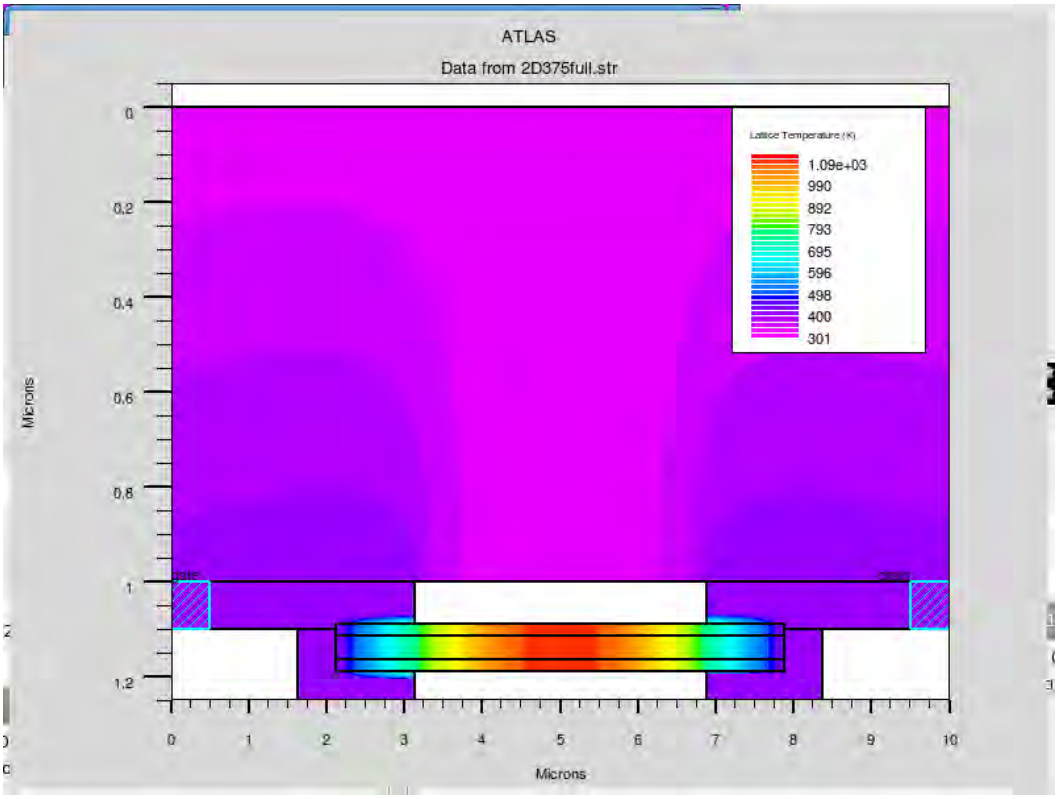

Figure 22. Heating in a suspended 3.75 µm CNF interconnect.

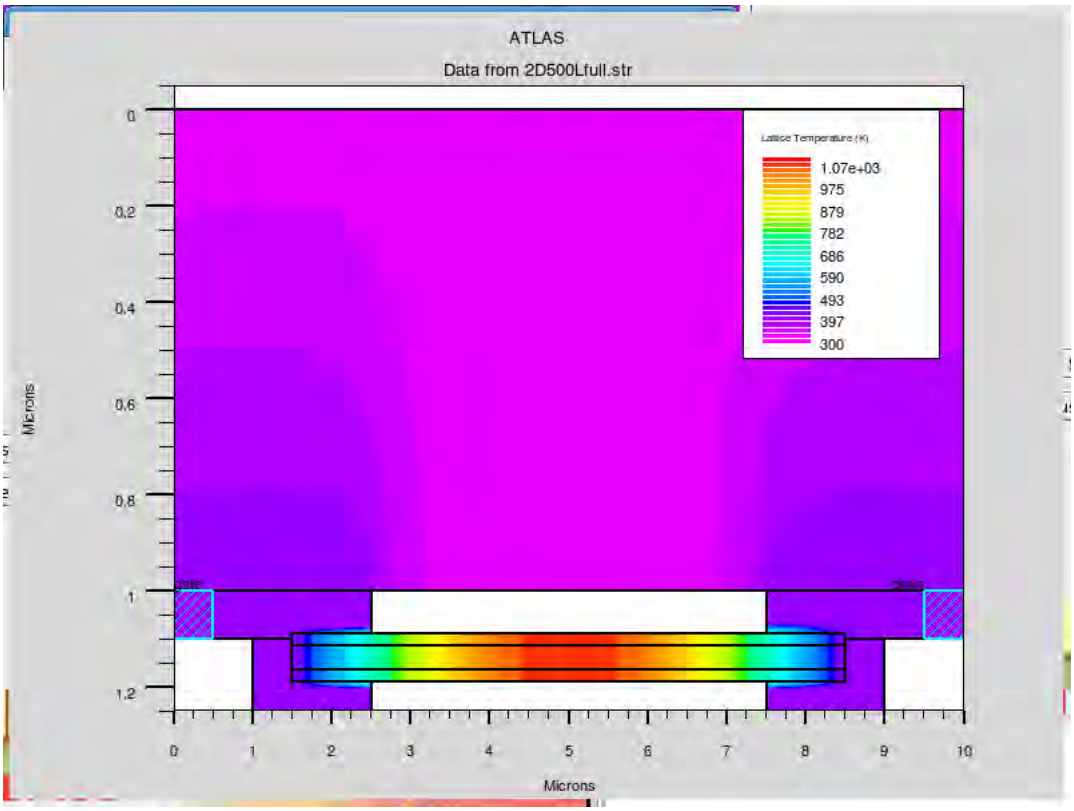

Figure 23. Heating in a suspended 5.00 µm CNF interconnect.

In the figures, the maximum temperature in Kelvins (K) varies from one figure to the next. This occurs as a result of different maximum voltage levels. All effort was made to stop the simulation near the experimental breakdown point of 900 K.

b. Effects of Length on J_{max}

In order to measure the current density and heating throughout the simulation, a probe point was placed at the center of the device in the bottom conducting region. The data shown in Figure 24 is an illustration of the lattice temperature versus the current density. As the voltage increased, the current density eventually reached a maximum point. Each line represents a different length of interconnect. The longest interconnect is displayed on the far left. In general, the maximum current density occurred between 900 and 1000 K. This is a good sign since the device would have failed within this region. Any data beyond the maximum current density is unrealistic and should be dismissed.

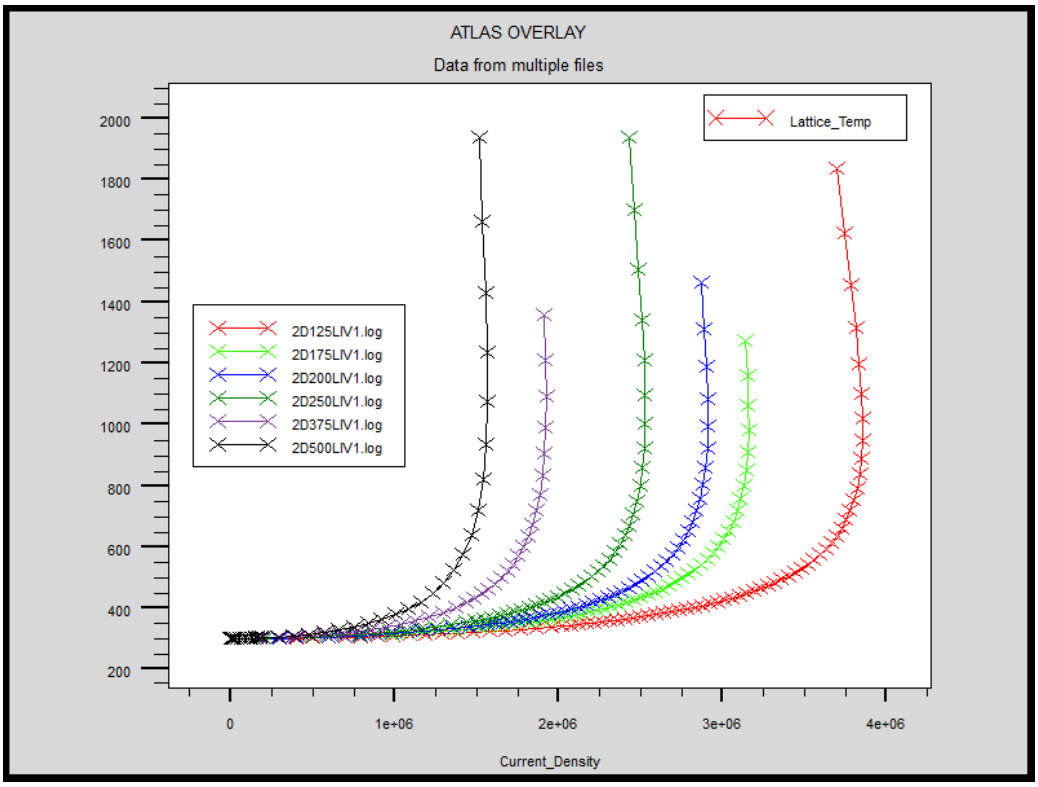

Figure 24. Temperature versus current density of suspended interconnects.

From Figure 24, it is difficult to tell where the maximum current density occurs. The individual curves were inspected more closely, as shown in Figure 25. In every case, the line had a maximum value that was represented by the bump seen in Figure 25. However, as just stated, any measurement above about 1000 K becomes unreliably because the device would have started to vaporize. The exact values obtained are compared to the SCU data in the next section.

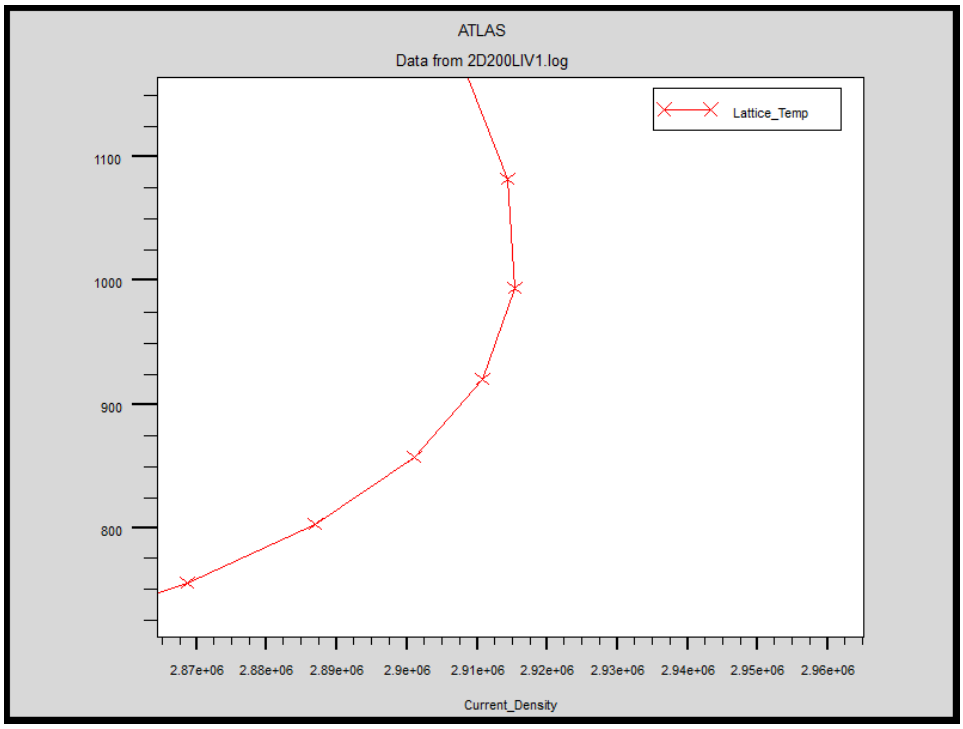

Figure 25. Close-up of temperature versus current density of a 2.00 CNF interconnect.

3. Comparison with SCU Data

The SCU data used for comparison is shown in Figure 13 in Chapter III. The fitted curve from this data follows [3, 5],

$$J = \frac{5.39}{L}, \tag{16}$$

where J is the current density and L is the length of the interconnect. In Table 6, the maximum current density from the fitted curve of the SCU experiments and the simulated data are shown. The graph shown in Figure 26 displays the data from Table 6.

Table 6. SCU J_{max} versus simulation J_{max}.

Length (μm)	1/L	SCU J_{max}	Simulation J_{max}
1.25	0.8	4.31×10^6	3.86×10^6
1.75	0.57	3.08×10^6	3.15×10^6
2.00	0.5	2.70×10^6	2.92×10^6
2.50	0.4	2.16×10^6	2.52×10^6
3.75	0.27	1.44×10^6	1.93×10^6
5.00	0.2	1.08×10^6	1.56×10^6

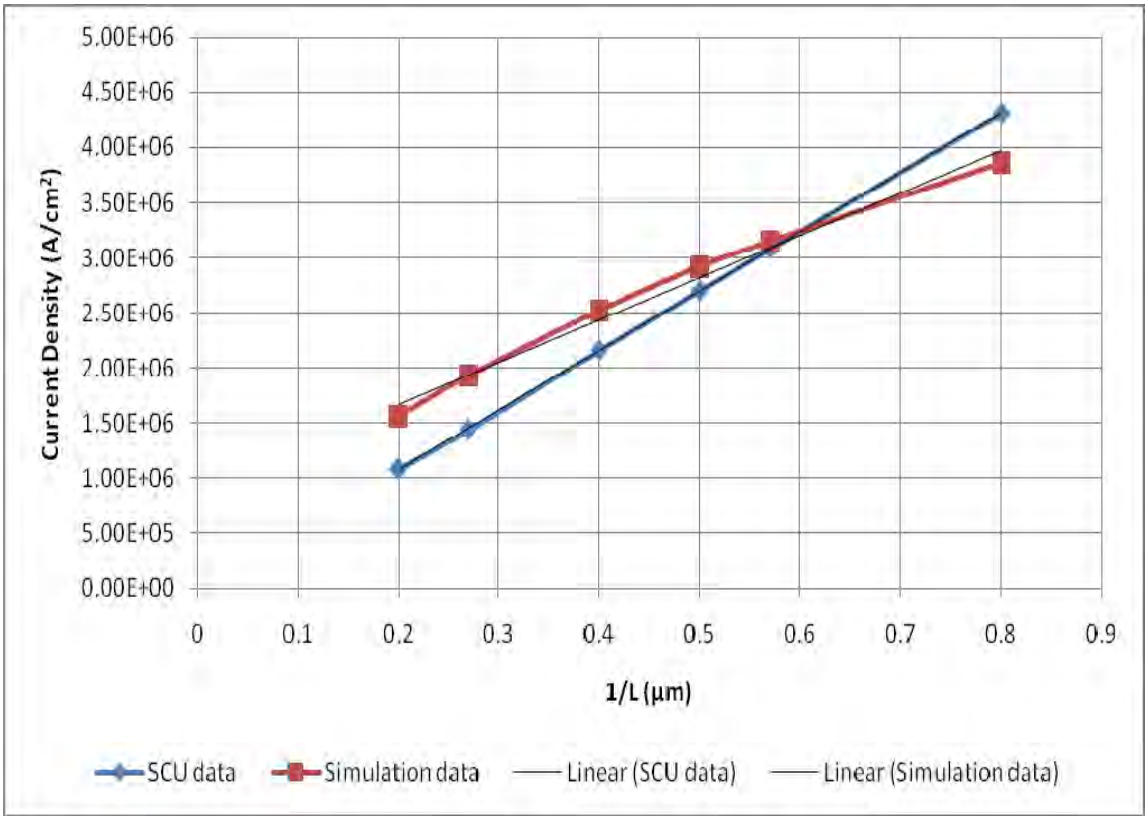

Figure 26. Current density versus inverse length of SCU fitted data and simulation results.

When compared to the SCU data, the simulation curve has a slightly higher recorded current density for longer CNFs. However, the slope of the line starts to match up with that of the SCU data. The density of states was found to have a direct effect on the maximum current density without having any effect on the slope of the curve. The error in the results may be a result of incorrect density of states for the CNF. Next, supported structures are examined.

B. 2D SUPPORTED W-AU CONTACT

1. Device Structures

A total of six device structures were tested for this set of data. Three different lengths of CNF, 1.25, 2.50, and 5.00 μm, were chosen. Each length of CNF was in contact with either 25% or 50% of the substrate, giving a total of six device structures for testing. As discussed in Chapter III, the CNF is connected to the substrate via a small block of SiO_2 material placed at the center of the CNF length.

2. Voltage Sweep

Just like the first set of test structures, all these devices had different maximum voltage values. Since the addition of the material allowed heat flow to substrate, the maximum voltages in the simulation needed to be increased. As in the first test, the voltage steps were kept the same for the simulation to create the best correlation.

a. Heating of Device

The heating of the six device structures are shown in Figures 27 through 32. The majority of the heat from the devices dispersed into the substrate through the small block of substrate material. In most simulations the contact with the substrate in the center of the device caused the hottest point on the device to move towards the contacts. This heating effect appears more clearly for longer CNF lengths. This implies there is a minimum amount of unsupported material needed to create two distinct hot points. In Figures 29 and 30, the 25% supported device has two distinct hot points, but

the 50% supported device does not. In order to better understand this heating effect, two extra probe points were placed at the center of the unsupported regions of each device. It was found that, as the length of the interconnect increases, the non-centered probe points heated up faster but eventually reached equilibrium with the centerpoint.

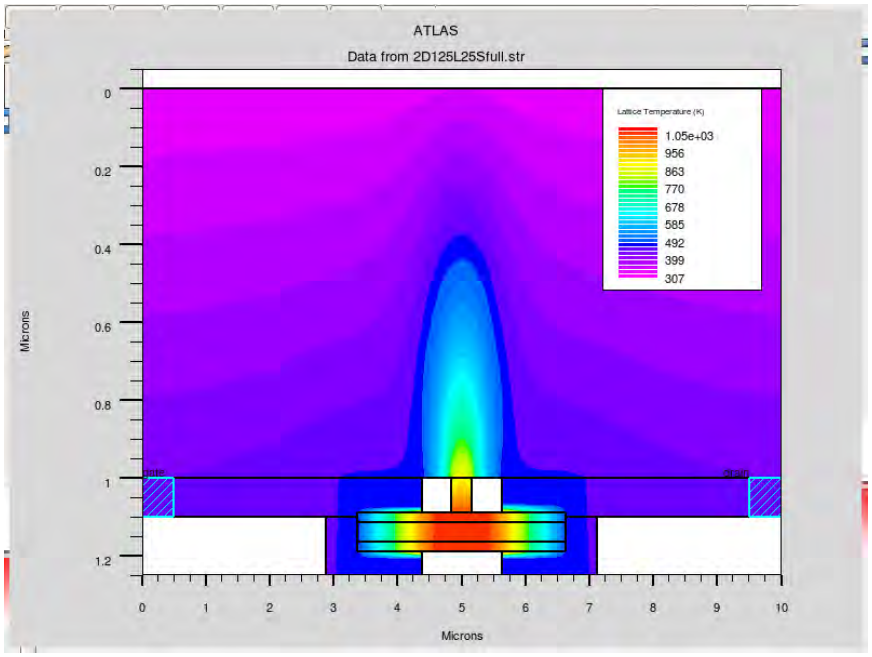

Figure 27. Heating in a 25% supported 1.25 µm CNF interconnect.

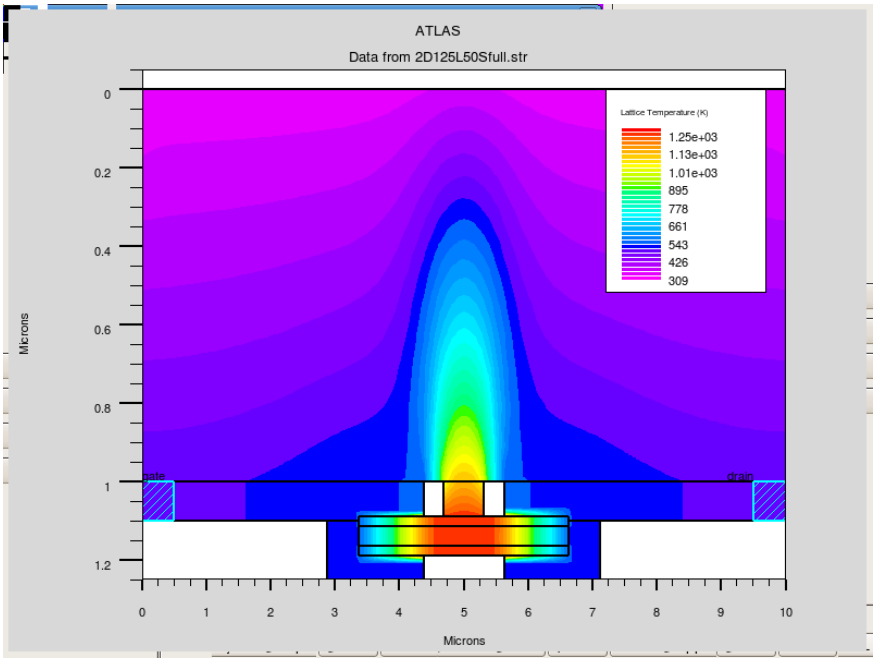

Figure 28. Heating in a 50% supported 1.25 µm CNF interconnect.

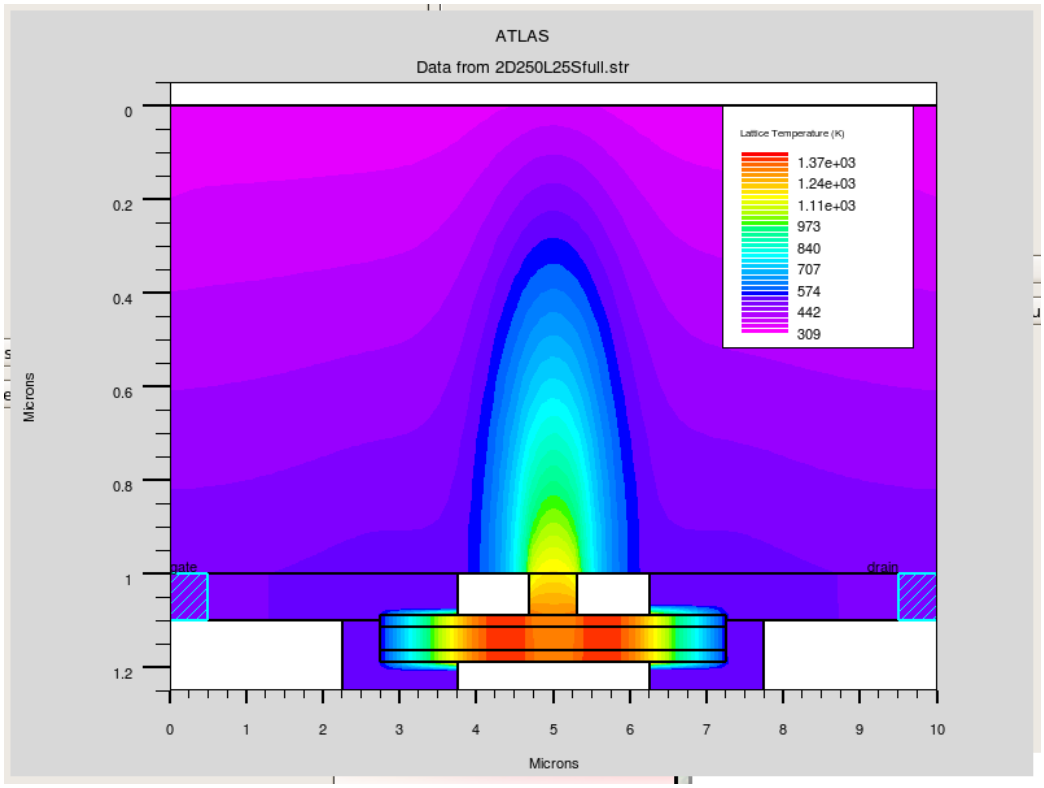

Figure 29. Heating in a 25% supported 2.50 µm CNF interconnect.

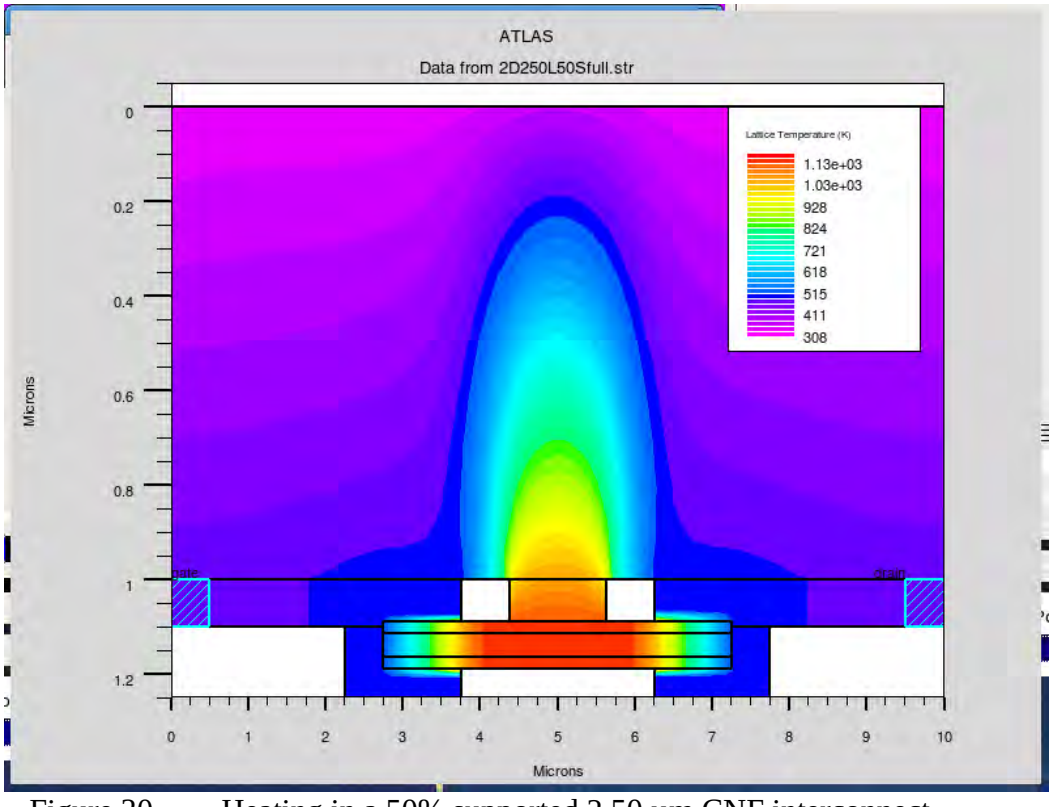

Figure 30. Heating in a 50% supported 2.50 µm CNF interconnect.

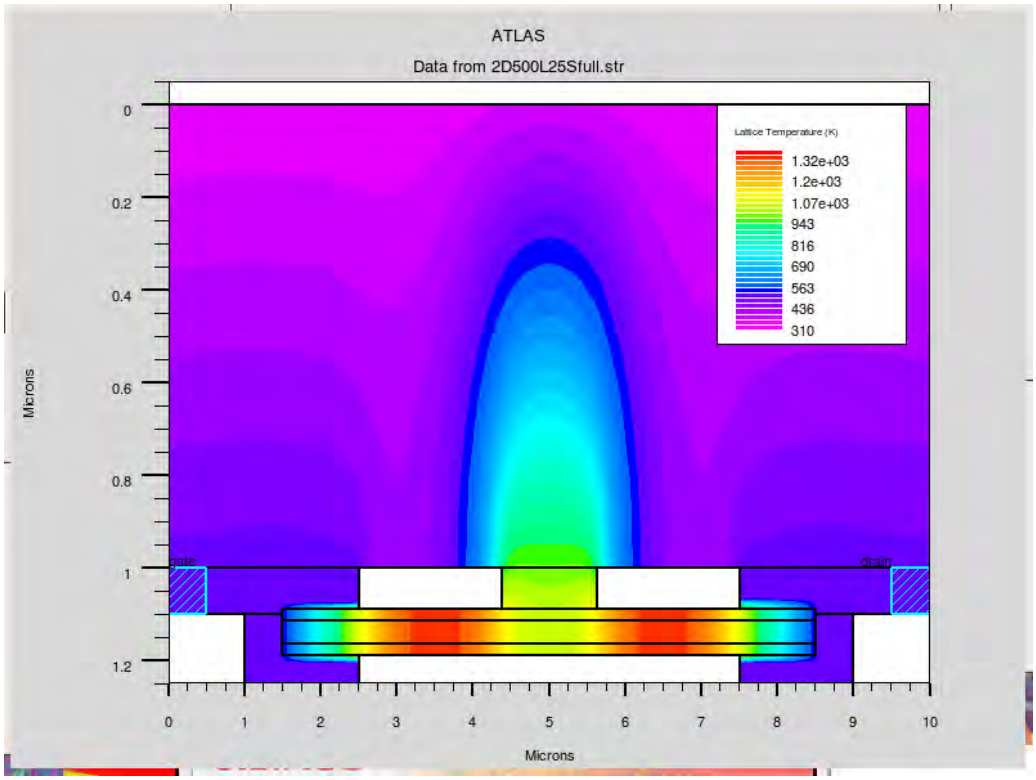

Figure 31. Heating in a 25% supported 5.00 µm CNF interconnect.

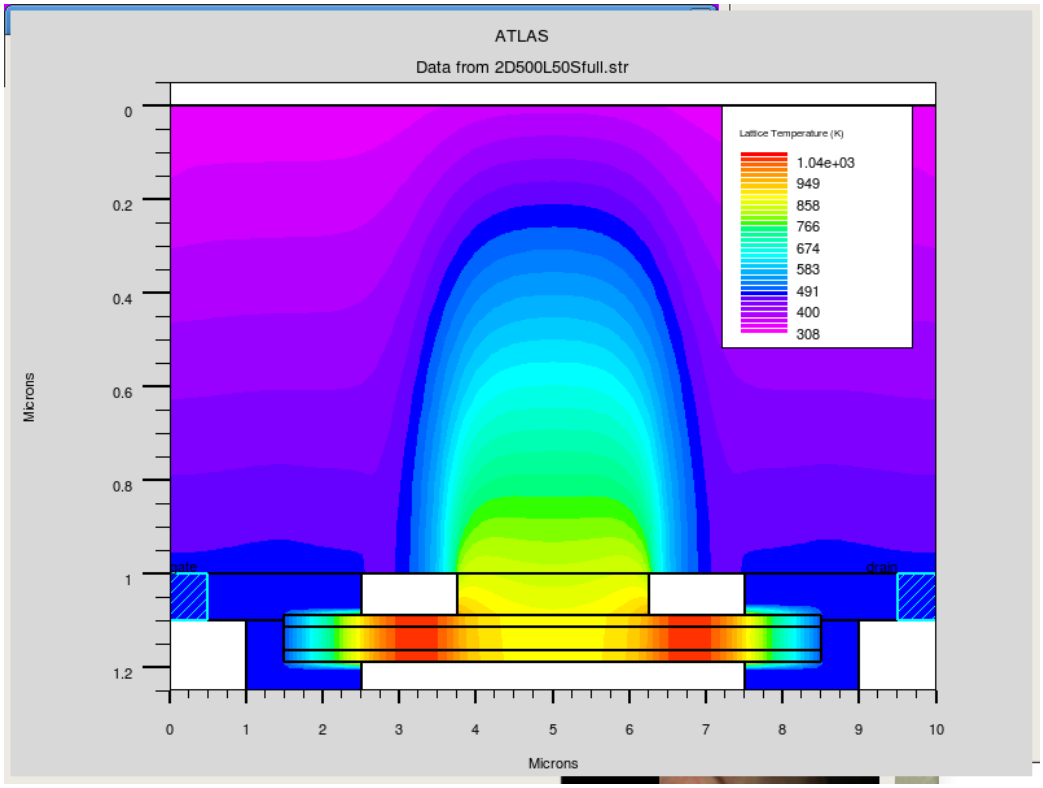

Figure 32. Heating in a 50% supported 5.00 µm CNF interconnect.

b. Effects of Support on J_{max}

It was determined that supporting any amount of the structure increased the maximum current density through the interconnect before failure. Temperature versus current density curves for 25% and 50% supported structures, respectively, are illustrated in Figure 33 and 34. The three different probe points are graphed for each of the structures. The shortest interconnect length is on the far right of the graph. For the 1.25 and 2.5 µm structures, the curves completely overlap, but for the 5.0 µm structure, the right and left probes exceed the temperature at the center probe. A graph of the 5.0 µm structure can be seen more clearly in Figure 35. In Figure 35, the global device temperature is also shown for comparison with the probes. It overlaps both the data lines for the left and right probes.

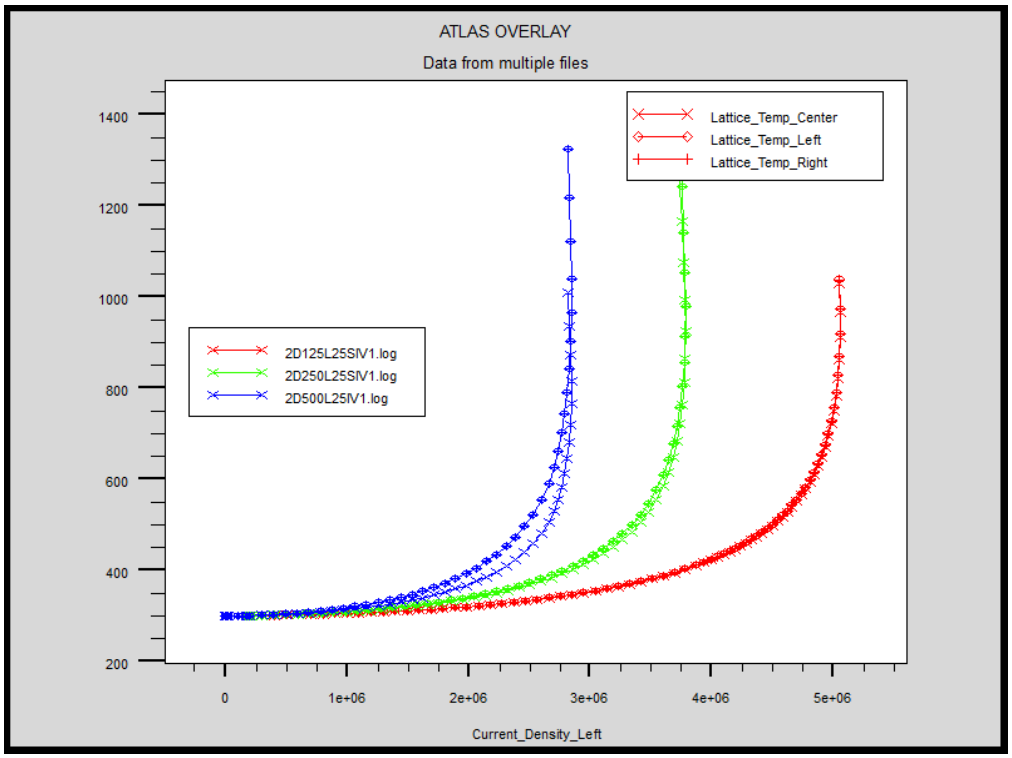

Figure 33. Temperature versus current density of 25% supported structures.

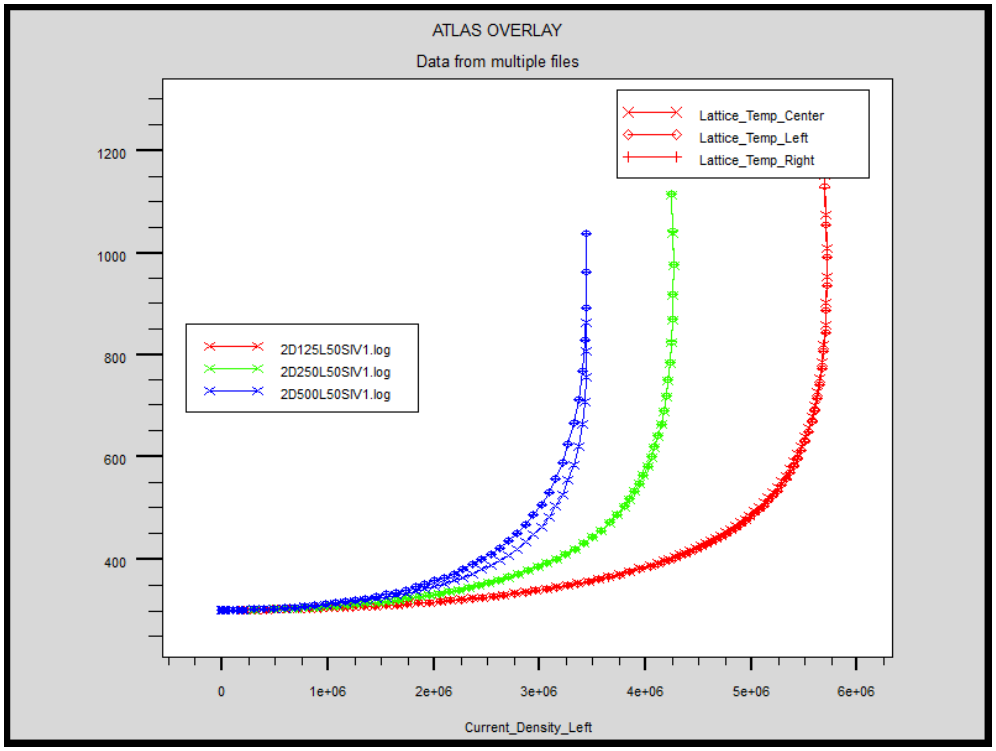

Figure 34. Temperature versus current density for 50% supported structures.

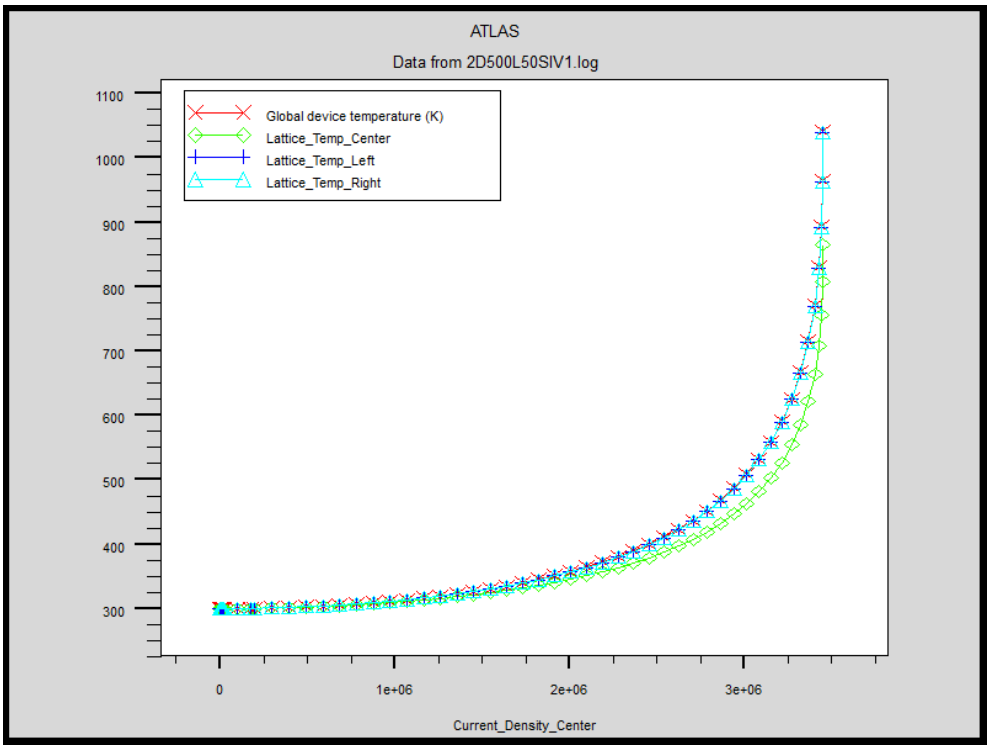

Figure 35. Temperature versus current density for 50% supported interconnects of 5.00 µm.

3. Comparison with SCU Data

From the data in Figure 13, there was no equation derived for the supported cases of the device, which means there was no exact data for comparison. Instead, the general curves shown in Figure. 13 were compared to the simulation curves. The maximum current densities for the various structures are contained in Table 7, and the graph of the values is shown in Figure 36.

Table 7. Simulated maximum current density data of supported structures.

Length (μm)	1/L	25% supported J_{max}	50% supported J_{max}
1.25	0.8	5.06 x 10^6	5.714 x 10^6
2.50	0.4	3.788 x 10^6	4.264 x 10^6
5.00	0.2	2.847 x 10^6	3.446 x 10^6

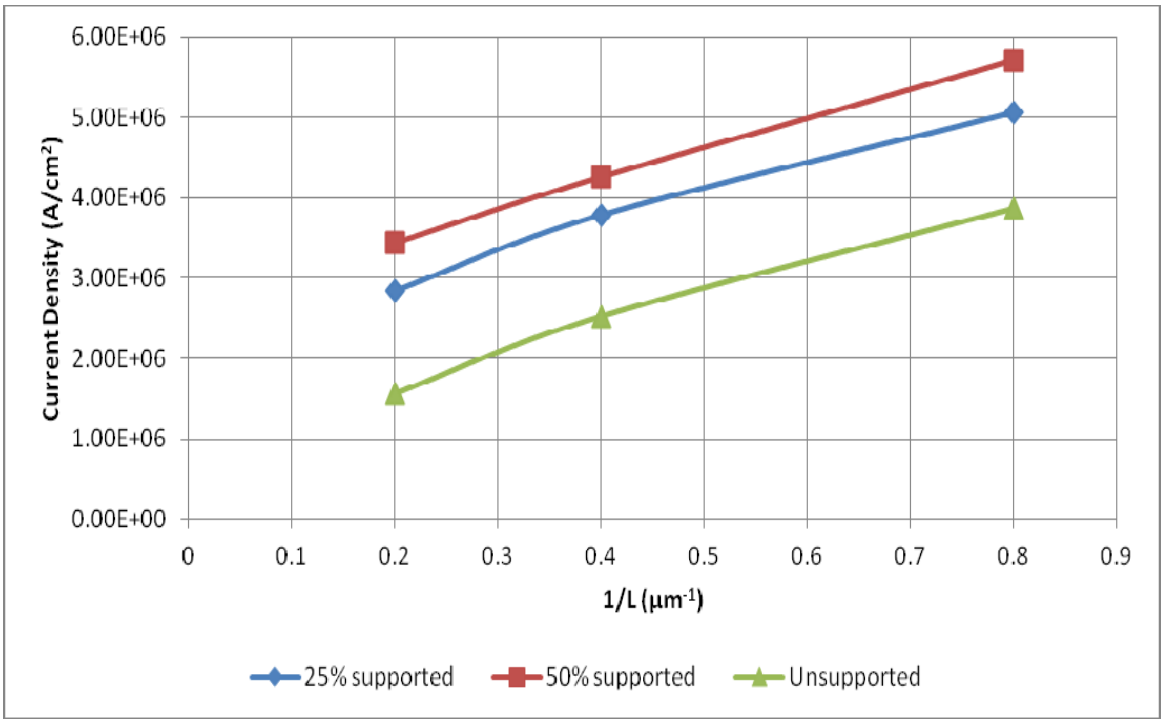

Figure 36. Current density versus inverse length of 25% and 50% supported structures. Lowest line represents data from suspended case.

From just a quick look at Figure 36, the supported cases produce higher maximum current densities. Unlike the predicted SCU data, the curves are nearly parallel to the suspended case. It should be noted that the SCU group did not test any short length CNFs in their experiments, and as such, the curve in Figure 13 is a prediction. The values achieved were higher than expected but still followed the basic trend of the SCU data. The benefit of adding more substrate support under the interconnect appears to diminish as more support is added. The heating effect in a 3D structure versus a 2D structure is examined in the next section.

C. 3D MODEL W-AU CONTACT

1. Device Structure

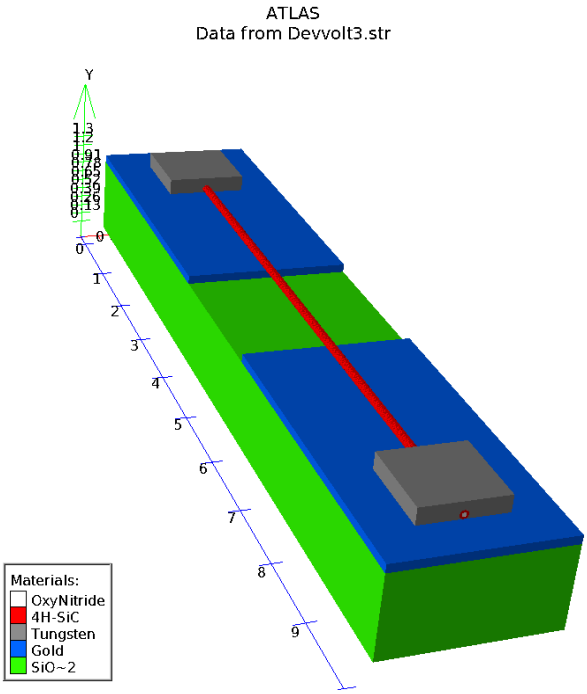

Figure 37. 3D structure of a 2.00 µm CNF interconnect.

The device structure for the 3D case differed slightly from the 2D models at the tungsten contact points. The contacts were placed at the very end of the CNF, which stretched for the entire length of the gold contacts. By placing the tungsten away from

the interconnect gap, the device model more accurately simulates a physical device. The finished structure is shown in Figures 37 and 38. The layers of CNF material and the contact are clearly illustrated in Figure 38.

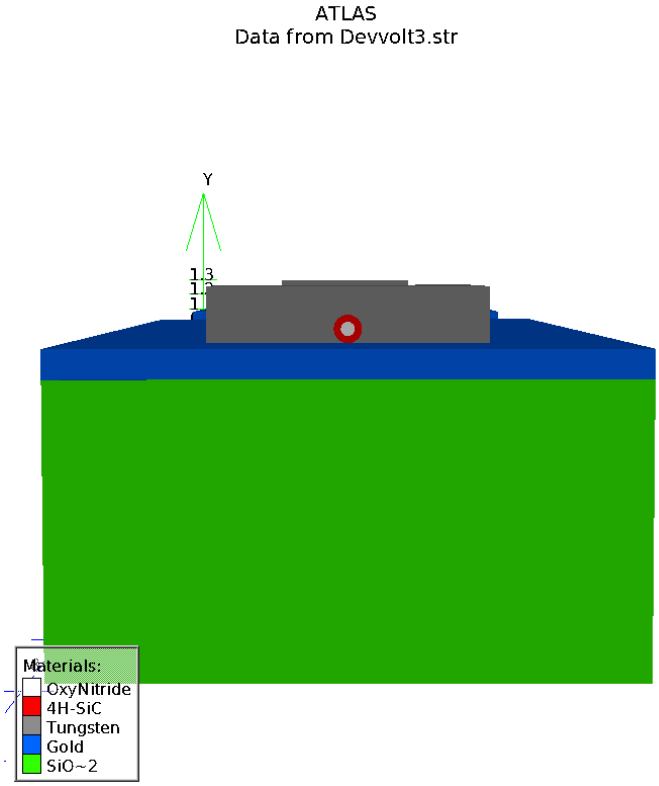

Figure 38. Side view of a 3D CNF interconnect.

2. Test Parameters

Originally, this thesis was meant to be done entirely with 3D structures; however, as testing progressed, it became clear that limitations in the Silvaco software would hinder that capability. As such, the 3D structure was biased as much as possible simply to show heating in the structure. All of the material parameters were kept the same and the device was run with a voltage sweep.

3. Comparison with 2D model

The resulting heating profile illustrates that the 2D model does not dissipate heat like the 3D model. The primary cause stems from the lack of contact between the two

conducting regions in the 2D model. In the 3D model, the heat can flow around the cylindrical surface of the structure and will accumulate as far away from the substrate and heat sinks as possible. The 3D profile picture is shown in Figure 39. A close-up on the active region, in Figure 40, illustrates how the heat accumulates at the top of the center of the CNF device.

In contrast, the 2D simulations produced a uniform heat gradient over the CNF materials. A close up on one edge of the hottest region of the CNF materials is illustrated in Figure 41. There seems to be no difference in the top and bottom of the CNF. The top of the image is the side closest to the substrate of the device.

The amount of material conducting differs between the 2D and the 3D models. In the 3D model, about 75% of the CNF is conducting material, whereas the 2D model has only 50% of the material conducting. This would lead to more heat being generated in a physical device versus heat being generated in a 2D model. However, the amount of contact material is much greater in the 3D model, which allows for greater amount of heat to dissipate into the contact. It is unclear as to which factor would contribute more.

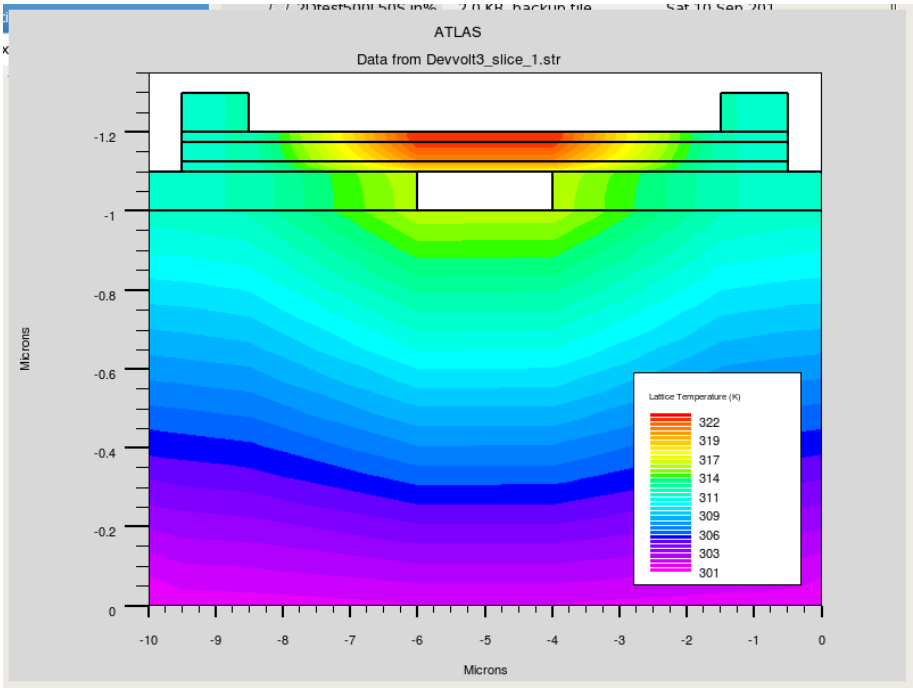

Figure 39. Cross-section view of heating in 2.00 µm 3D CNF interconnect.

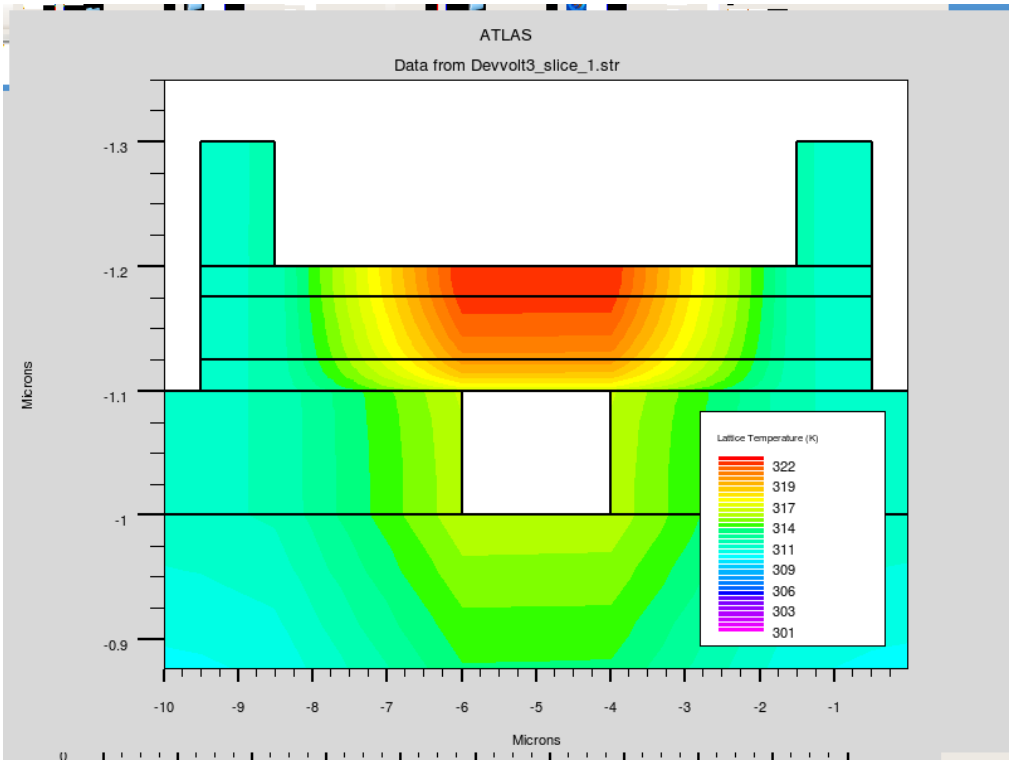

Figure 40. Close-up of heating in a 2.00 µm 3D CNF interconnect.

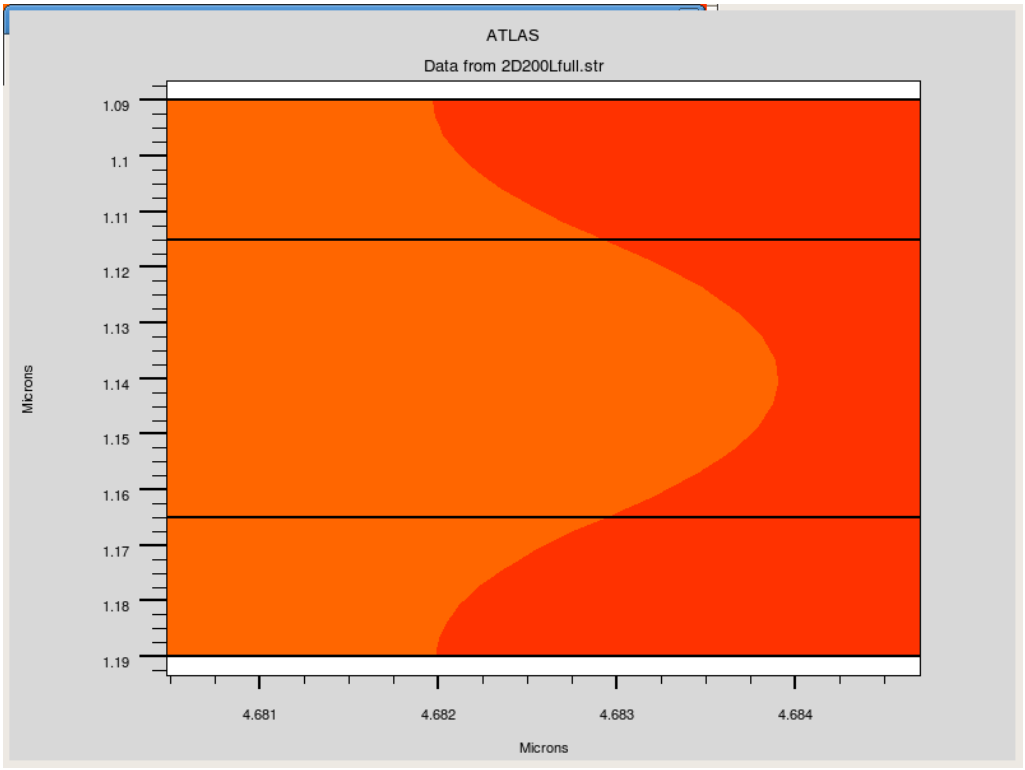

Figure 41. Close-up of heating across CNF regions in a 2D simulation of a 2.00 µm interconnect.

D. CHAPTER SUMMARY

In this chapter, the experimental data was presented and analyzed. The 2D simulations provided data that closely approximated the SCU experimental data. The maximum current density increased as the length of interconnects shrank. Also, the addition of substrate support material increased the average maximum current density of interconnects. However, it was found that the heating in the 2D simulations did not match the heating within a 3D structure. This implies there might be an error in the physics for the 2D model simulation.

In the next chapter, the conclusions drawn from the experiments are presented. In addition, recommendations for improving the current model and possible future projects are discussed.

THIS PAGE INTENTIONALLY LEFT BLANK

V. CONCLUSION AND RECOMMENDATIONS

A. CONCLUSION

A method to simulate the heating and maximum current density for a CNF interconnect was presented in this thesis. The simulation provides a first step towards creating a complete model of a CNF interconnect that has the ability to accept any input characteristics and accurately model the internal physics. Further, the simulation demonstrated the ability to estimate the maximum current density with only marginal error. The error present could possibly be removed by better definition of the material characteristics and physics of the CNF material.

The results from the 2D simulations provided data that closely matched the SCU experiments. The most important factor that contributed to the maximum current density was determined to be the density of states of the CNF material. Any error in the results could be attributed to a miscalculation of the density of states. Also, the contact resistances were found to contribute little to the maximum current density unless the order of magnitude changed. As long as the resistances remained under 10 kΩ, there was little to no change to the current density curve.

A significant limitation of the model in its current form is the inability to apply constant voltage or current over time. If the current model is driven over time, the device heats up too quickly for the solver to converge. Future work would involve rectifying this problem and comparing the results to the constant current experiments done at SCU.

As work progresses, it would be valuable to have the ability to directly compare current metal interconnects versus CNF interconnects. As devices shrink, Cu interconnects are becoming a greater reliability issue. With this model, it would be possible to study the advantages of integrating CNFs in a large scale manner.

The next section contains some recommendations for advancing the functionality of the device model. Also, some issues that arose during the process are discussed.

B. RECOMMENDATIONS

During this project, it became quite clear that Silvaco ATLAS can be very limiting when creating custom materials and complex geometric structures. If one were to attempt a similar project that required creating a new material or complex geometry, ATLAS is not recommended. A wise alternative to ATLAS would have been COMSOL. COMSOL is a finite element solver that can simulate a wider variety of physics problems than ATLAS.

ATLAS is particularly good for analyzing characteristics of well-defined materials, such as silicon or gallium nitride. Since there is no way to make an entirely new material, an existing material needs to be modified in order create a material with the characteristics needed. This means that all the parameters of the material need to be closely analyzed so that no errors occur within the simulation.

Also, when constructing a structure with complex geometries, ATLAS takes considerably longer to simulate the structure. The mesh around the interfaces of complex geometries needs to be very well defined, which leads to longer simulation times.

APPENDIX. DECKBUILD INPUT CODE

```
##################################################################
#       Author: Jason Brunton                                    #
#       Naval Postgraduate School                                #
#       13 September 2011                                        #
#                                                                #
#       CNF interconnect Simulation file                         #
#                                                                #
#       Programs:                                                #
#               Deckbuild™                                       #
#               Atlas™                                           #
#               DevEdit™                                         #
##################################################################


go atlas

mesh infile=2D175L2.str conductor

# Contact Parameters
contact name=gate resistance=5e3
contact name=drain resistance=5e3

# Band Parameters
material material=OxyNitride permittivity=5.4
material material=4H-SiC permittivity=5.4
material material=4H-SiC eg300=.026
material material=4H-SiC NC300=3.0e17 NV300=3.0e17
material material=4H-SiC NC.F=0 NV.F=0

# Recombination Parameters
material material=4H-SiC taun0=0 taup0=0 etrap=0
material material material=4H-SiC augn=0 augp=0
material material=4H-SiC augkn=0 augkp=0
material material=4H-SiC kaugcn=0 kaugcp=0
material material=4H-SiC kaugdn=0 kaugdp=0
material material=4H-SiC copt=0

# Thermal Parameters
material material=4H-SiC tcon.const tc.const=0.12
material=4H-SiC nsrhn=0 nsrhp=0
material material=4H-SiC ksrhtn=0 ksrhtp=0
material material=4H-SiC ksrhcn=0 ksrhcp=0
```

```
material material=4H-SiC ksrhgn=0 ksrhgp=0
material material=4H-SiC HC.A=1.75 HC.B=0 HC.D=0
material material=OxyNitride tcon.const tc.const=0.12 HC.A=1.75

mobility material=4H-SiC mun0=100000 mup0=100000

models srh joule.heat fermi auger lat.temp gr.heat print

thermcontact num=1 x.min=0.0 x.max=10.0 y.min=0 y.max=0.1 alpha=1.4e3

method block newton tol.ltemp=1.0 climit=1e-4

solve init
solve previous
save outfile=2D175Linit.str

log outfile=2D175LIV1.log

probe name=Current_Density J.Total x=5.0 y=1.1
probe name=Lattice_Temp Lat.temp x=5.0 y=1.1

solve vgate=0.001

solve vgate=0.005 vstep=0.03 vfinal=0.095 name=gate

solve vgate=0.10 vstep=0.40 vfinal=0.9 name=gate

solve vgate=1.0 vstep=0.5 vfinal=7.0 name=gate

solve vgate=7.5 vstep=0.25 vfinal=18.75 name=gate
save outfile=2D175Lfull.str

quit
```

LIST OF REFERENCES

[1] R. Saito, G. Dresselhaus, and M. S. Dresselhaus, *Physical Properties of Carbon Nanotubes*, Imperial College Press, London, 1998.

[2] T. Saito, T. Yamada, D. Fabris, H. Kitsuki, P. Wilhite, M. Suzuki, and C. Y. Yang, "Improved contact for thermal and electrical transport in carbon nanofiber interconnects," *Appl. Phys. Lett.*, vol. 93 (10), no. 102108, 2008.

[3] T. Yamada, T. Saito, D. Fabris, and C.Y. Yang, "Transport Phenomena in Carbon Nanostructures," *IEEE International Nanoelectronics Conference*, Hong Kong, Paper KS420, 2010.

[4] T. Yamada, H. Yabutani, T. Saito, and C. Y. Yang, "Temperature dependence of carbon nanofiber resistance," *Nanotechnology*¸ Vol. 21, pp. 265−707, 2010.

[5] T. Yamada, T. Saito, D. Fabris, and C. Y. Yang, "Electrothermal Analysis of Breakdown in Carbon Nanofiber Interconnects," *IEEE Elec. Dev. Lett.*, vol. 30 (5), pp. 469−471, 2009.

[6] H. Yabutani, T. Yamada, T. Saito, and C. Y. Yang, "Joule-heating dependence of carbon nanofiber resistance," *IEEE Nanotechnology Materials and Devices Conference*, Traverse City, MI, pp. 166−168, 2009.

[7] H. Kitsuki, T. Yamada, D. Fabris, J. R. Jameson, P. Wilhite, M. Suzuki, and C. Y. Yang, "Length dependence of current-induced breakdown of carbon nanofibers," *Appl. Phys. Lett.*, vol. 92, no. 173110, 2008.

[8] Q. Ngo, T. Yamada, K. Gleason, M. Suzuki, H. Kitsuki, A. M. Cassell, and C. Y. Yang, "Electrothermal Transport in Carbon Nanostructures," Proceedings of the ULSI Process Integration 6 Symposium, Electrochemical Society Meeting, Vienna; *ECS Trans*., vol. 25, issue 7, pp. 487−493, 2009.

[9] S. Maeda, T. Yamada, P. Wilhite, H. Yabutani, T. Saito, and C. Y. Yang, "W-deposited contacts with carbon nanofiber using focused ion and electron beams," *IEEE Nanotechnology Materials and Devices Conference*, Monterey, CA, pp. 125−127, 2010.

[10] T. Yamada, T. Saito, M. Suzuki, P. Wilhite, X. Sun, N. Akhavantafti, D. Fabris, and C. Y. Yang, "Tunneling between carbon nanofiber and gold electrodes," *J. Appl. Phys.*, vol. 107, no. 044304, 2010.

[11] T. Yamada, F. R. Madriz, and C. Y. Yang, "Inductance in One-Dimensional Nanostructures," *IEE Transactions on Electron Devices*, vol. 56, p. 1834−1839, 2009.

[12] S. Iijima, “Helical Microtubules of Graphitic Carbon,” *Nature*, vol. 354, pp. 56−58, 1991.

[13] S. Iijima and T. Ichihashi, “Single-shell Carbon Nanotubes of 1-nm diameter,” *Nature*, vol. 363, pp. 603−605, 1993.

[14] M. S. Dresselhaus, G. Dresselhaus, and R. Saito, “Physics of Carbon Nanotubes,” *Carbon*, vol. 33, no. 7, pp. 883−891, 1995.

[15] Q. Ngo, T. Yamada, M. Suzuki, Y. Ominami, A. M. Cassell, J. Li, M. Meyyappan, and C. Y. Yang, “Structural and Electrical Characterization of Carbon Nanofibers for Interconnect Via Applications,” *IEEE Trans. Nano.*, vol. 6, no. 6, pp. 688−695, 2007.

[16] C. V. Thompson, “Carbon nanotubes as Interconnects: Emerging Technology and Potential Reliability Issues,” *Reliability Phys. Sym.*, pp. 368−376, 2008.

[17] J. Li, A. Cassell, H. T. Ng, R. Stevens, J. Han, and M. Meyyappan, “Bottom-up approach for carbon nanotube interconnects,” *Appl. Phys. Lett.*, vol. 82, no. 15, pp. 2491−2493, 2003.

[18] N. Srivastava, R. V. Joshi, and K. Banerjee, “Carbon Nanotube Interconnects: Implications for Performance, Power Dissipation and Thermal Management,” *Electron Devices Meeting. IEDM Technical Digest*, pp. 249−252, 2005.

[19] N. Kuruvilla and J. P. Raina, “Statistical Latency Analysis of Carbon nanotube Interconnects due to Contact Resistance Variations,” *Inter. Conf. Microelectronics*, pp. 296−299, 2008.

[20] A. Srivastava, Y. Xu, and A. K. Sharma, “Carbon nanotubes for next generation very large scale integration interconnects,” *J. Nanophotonics*, vol. 4, no. 041690, 2010.

[21] Silvaco, Inc. *Atlas user’s manual*. Santa Clara, CA: Silvaco, Inc., 2010.

INITIAL DISTRIBUTION LIST

1. Defense Technical Information Center
   Ft. Belvoir, Virginia

2. Dudley Knox Library
   Naval Postgraduate School
   Monterey, California

3. Engineering and Technology Curricula Office, Code 34
   Naval Postgraduate School
   Monterey, California

4. Chairman, Code EC (590)
   Department of Electrical and Computer Engineering
   Naval Postgraduate School
   Monterey, California

5. Professor Todd R. Weatherford, Code EC (590)/Wt
   Department of Electrical and Computer Engineering
   Naval Postgraduate School
   Monterey, California

6. Professor Sebastion Osswald, Code PH
   Naval Postgraduate School
   Monterey, California

7. Jason A. Brunton, Code EC (590)
   Department of Electrical and Computer Engineering
   Naval Postgraduate School
   Monterey, California